ORNL/TM-13444

Metals and Ceramics Division

Engineering Materials Section

APPLICATION OF HIGH–PERFORMANCE COMPUTING TO AUTOMOTIVE DESIGN AND MANUFACTURING COMPOSITE MATERIALS MODELING TASK TECHNICAL MANUAL FOR CONSTITUTIVE MODELS FOR GLASS FIBER-POLYMER MATRIX COMPOSITES

Srdan Simunovic and Thomas Zacharia

The Oak Ridge National Laboratory

Date Published: December 1997

Research was sponsored by the U.S. Department of Energy under contract DE-AC05-96OR22464 with Lockheed Martin Energy Research Corporation.

Prepared by the
OAK RIDGE NATIONAL LABORATORY
Oak Ridge, Tennessee 37831
managed by
LOCKHEED MARTIN ENERGY RESEARCH CORP.
for the
U.S. DEPARTMENT OF ENERGY
under Contract No. DE-AC05-96OR22464

CONTENTS

1 INTRODUCTION **1**

2 DAMAGE MECHANICS **3**

3 ANISOTROPIC DAMAGE MODEL FOR UNIDIRECTIONAL FIBER COMPOSITES **6**

4 HYDROSTATIC PRESSURE DEPENDENT DAMAGE MODEL **11**

5 DAMAGE MODEL WITH STRAIN TENSOR SPLIT **16**

6 CRUSH FRONT MODEL **19**

7 NUMERICAL RESULTS **22**

7.1 Damage Model for Unidirectional Fiber Composites 22

7.2 Hydrostatic Pressure–Dependent Damage Model 30

7.3 Damage Model with Strain Tensor Split 34

8 MATERIAL DATA INPUT FORMATS FOR DYNA3D **44**

8.1 Material 52: Anisotropic Damage Model 44

8.2 Material 54: Hydrostatic Pressure Dependent Damage Model 45

8.3 Material 53: Damage Model with Strain Tensor Split 47

9 CONCLUSIONS **48**

10 REFERENCES **49**

LIST OF FIGURES

1 Weighted crush front propagation 21
2 Drop Tower Test Configuration 23
3 Deformed CSM Specimen after Drop Tower Test 24
4 Material 52, Tube Deformation, 0^o Fibers 25
5 Material 52, Tube Deformation, 0^o Fibers 26
6 Material 52, Tube Deformation, 90^o Fibers 27
7 Material 52, Tube Deformation, 90^o Fibers 28
8 Material 5, Barrier Force 29
9 Material 54, Tube Deformation 1 31
10 Material 54, Tube Deformation 2 32
11 Material 54, Barrier Force 33
12 Material 53, Determination of m Value from Experiments 36
13 Material 53, Coarse Mesh 37
14 Material 53, Coarse Mesh, Deformation Sequence 1 38
15 Material 53, Coarse Mesh, Deformation Sequence 2 39
16 Material 53, Coarse Mesh, Bottom View 40
17 Material 53, Fine Mesh 41
18 Material 53, Fine Mesh, Bottom View 42
19 Material 53, Barrier Force 43

ACKNOWLEDGEMENTS

Research was sponsored by the U.S. Department of Energy, Assistant Secretary for Energy Efficiency and Renewable Energy, Office of Transportation Technologies, Lightweight Materials Program, and by the U.S. Department of Energy Defense Programs, Assistant Secretary, Technology Management Group, Technology Transfer Initiative, under contract DE-AC05-96OR22464 with Lockheed Martin Energy Research Corporation.

APPLICATION OF HIGH–PERFORMANCE COMPUTING TO AUTOMOTIVE DESIGN AND MANUFACTURING COMPOSITE MATERIALS MODELING TASK TECHNICAL MANUAL FOR CONSTITUTIVE MODELS FOR GLASS FIBER-POLYMER MATRIX COMPOSITES

Srdan Simunovic and Thomas Zacharia

ABSTRACT

This report provides a theoretical background for three constitutive models for a continuous strand mat (CSM) glass fiber-thermoset polymer matrix composite. The models were developed during fiscal years 1994 through 1997 as a part of the Cooperative Research and Development Agreement, "Application of High–Performance Computing to Automotive Design and Manufacturing." The full derivation of constitutive relations in the framework of the continuum damage mechanics is presented. The developed models have been implemented in the computer program DYNA3D and have been used for the simulation and impact analysis of CSM composite tubes. The analysis of simulation and experimental results show that the model based on strain tensor split yields the most accurate results of the three implemented models. The parameters used in the models and their derivation from the physical tests are documented. The input format for the computer program DYNA3D in the framework of user material model routines is provided.

1. INTRODUCTION

Composites Materials Modeling is a part of the Cooperative Research and Development Agreement (CRADA), "Application of High–Performance Computing to Automotive Design and Manufacturing" that has been established among Argonne National Laboratory in Argonne, Illinois; Lawrence Livermore National Laboratory in Livermore, California; Los Alamos National Laboratory in Los Alamos, New Mexico; Oak Ridge National Laboratory in Oak Ridge, Tennessee; Sandia National Laboratory in Albuquerque, New Mexico; Chrysler Corporation; Ford Motor Company; and General Motors Corporation. The terms of the CRADA can be found in Reference 1.

This report provides technical documentation and a user's manual for the computer implementation of the constitutive material models developed at ORNL for a continuous strand mat (CSM) glass fiber-thermoset polymer matrix composite. The models were developed for the simulation of thin plate and shell composite structures under impact loading. The overview of the literature and the modeled deformation mechanisms are documented in the accompanying report.[2] This report supersedes the working draft CRADA report.[3] Chapter 2 gives a short overview of the damage mechanics principles essential to understanding the developed material models. Chapters 3, 4 and 5 are devoted to the three developed material models, respectively. The first model, *Anisotropic Damage Model*, has been developed for unidirectional fiber composites and has been used mainly as a benchmark for the two following isotropic models, *Hydrostatic Pressure Dependent Damage Model* and *Damage Model with Strain Tensor Split*. Damage Model with Strain Tensor Split has been shown to provide the best results in simulation of the deformation of the CSM composite tubes. The constitutive model chapters are followed by a chapter on crush front modeling which details the developments on simulation of the progressive material degradation ahead of the impact zone primarily caused by advancement of interply cracks. However, because of the difficulties with the experimental quantification and separation of this effect from other deformation processes, as well as with the respective theoretical approach, further development of the crush front model has been directed towards integration of the interply cracking effects into material models directly. Chapter 7 deals with computational simulations of the various

tube impacts and their comparison with experimental data. Chapter 8 provides the format and typical properties for the material model implementation in DYNA3D. Conclusions and recommendations for practical applications to automotive simulations and design are given in the final chapter.

2. DAMAGE MECHANICS

The structures made of glass fiber-polymer matrix composites show inherently brittle behavior. The principal mechanism for energy dissipation is formation of internal surfaces that are associated with the loss of interatomic bonds in the material that is referred to as damage. Damage mechanics theory models such a behavior by relating defect nucleation and growth in material to its macroscopic response. The damage in the CSM composites can be generally observed in the three constituent phases: glass fiber, polymer matrix, and their interface. Each of the phases has numerous damage mechanisms that may interact with damage from other phases depending on both intrinsic (material) and extrinsic (geometry, loading) effects. Modes of damage interaction are difficult to quantify, and a considerable number of assumptions usually needs to be made to yield a tractable model. The models developed in this study follow the basic steps of the damage mechanics framework that are subsequently outlined. The energy dissipation mechanisms in the material are described by material internal variables, ω_i, that reflect average material degradation and damage evolution. Thorough theoretical treatment of damage mechanics can be found in standard textbooks e.g., Reference 4. Only the main relations will be reviewed here to provide a complete set of equations for the reader.

One of the first decisions to be made is to choose the equivalency principle for the damage model. The damaged material state can be described using the equivalency principles that either: (a) equate the strain state of the damaged and undamaged material, (b) equate the stress state of the material, or (c) equate the energy of the damaged and fictitious undamaged material. The methodology used in this work is based on the strain equivalence mainly because of its computational efficiency in the framework of explicit time integration computer programs such as DYNA3D.

Because the nature of deformation and geometry of the structures that are to be modeled, all of the developed CSM composite models start from the following assumptions:

1. All nonlinear effects of constitutive behavior are attributed to damage. Plastic deformations are negligible.

2. Unloading and reloading do not produce damage in the material.

3. Damage depends on the resulting tensile and compressive states.

4. The model is developed for shell structures for which the state of plane stress is prevalent.

Assumptions 1 and 2 restrict the functional dependence of the material's free energy as

$$\Psi = \Psi\left(\epsilon, \omega\right) \quad , \tag{2.1}$$

where ϵ denotes a strain tensor and ω represents damage descriptors (variables). In the developed models, the unilateral nature of the damage has been modeled by expressing the free energy into separate parts that correspond to different damage mechanisms. Therefore, the energy associated with the particular damage mode, and its evolution, can be easily identified and derived from Eq. (2.1).

Stress tensor is derived from the free energy as

$$\sigma = \frac{\partial \Psi\left(\epsilon, \omega\right)}{\partial \epsilon} \quad . \tag{2.2}$$

The associated thermodynamics force to damage variables, ω, can be defined as

$$Y = -\frac{\partial \Psi\left(\epsilon, \omega\right)}{\partial \omega} \quad , \tag{2.3}$$

which controls the kinematics of the damage evolution. To account for the nature of irreversibility during damage processes, the following criteria for damage evolution are proposed:

$$g_\omega = \hat{R}(Y) - r(\omega) \leq 0 \quad , \tag{2.4}$$

where R denotes the function describing the current damage state and r denotes the damage strengthening threshold at the current time. Equation (2.4) can be used for modeling the initiation of the damage as well as initial damage in the material as the result of the material processing conditions. Equation (2.4) also makes it possible to restrict the damage evolution to the increased loading only.

To achieve a good numerical efficiency, all the corresponding models have been formulated as functions of the strain tensor.

3. ANISOTROPIC DAMAGE MODEL FOR UNIDIRECTIONAL FIBER COMPOSITES

The model was originally developed for modeling of the impact of composite tubes in References 5–7. The composite is assumed to consist of unidirectional laminae plies. The damage mechanisms that lead to material failure have been identified in References 5 and 8. These mechanisms are matrix cracking transverse to fibers, transverse matrix crushing, fiber breakage, fiber buckling, and matrix failure in the fiber direction. These damage modes are modeled using three independent damage variables, $\omega_{\parallel}$, $\omega_{\perp}$, and ω_s, for the direction parallel to the fibers, direction transverse to the fibers, and shearing in the plane of the laminae, respectively.

The strain energy for these damage mechanisms can then be written in the following form:

$$\begin{aligned}\Psi &= \frac{1}{2c}\left[(1-\omega_{\parallel})E_{\parallel}\epsilon_{11}^2 + (1-\omega_{\parallel})(1-\omega_{\perp})(\nu_{21}E_{\perp} + \nu_{12}E_{\parallel})\epsilon_{11}\epsilon_{22} + (1-\omega_{\perp})E_{\parallel}\epsilon_{22}^2\right] \\ &\quad +2(1-\omega_s)G\epsilon_{12}^2 \quad , \end{aligned} \tag{3.1}$$

where

$$c = 1 - (1-\omega_{\parallel})(1-\omega_{\perp})\nu_{12}\nu_{21} \quad , \tag{3.2}$$

$$\nu_{12}E_{\parallel} = E_{\perp}\nu_{21} \quad , \tag{3.3}$$

indices $\parallel$ and $\perp$ denote the values in the direction parallel and transverse to fibers, respectively. Indices 1 and 2 denote the principal coordinate directions. Symbols E, G, and μ denote the Young's modulus, shear modulus, and the Poisson's ratio of the undamaged laminae, respectively. The stress-strain relation of the damaged ply can be written in the

standard form using Eq. (2.2) as

$$\left\{ \begin{array}{c} \sigma_{11} \\ \sigma_{22} \\ \sigma_{12} \end{array} \right\} = \left[\begin{array}{ccc} (1-\omega_{\|})E_{\|} & (1-\omega_{\|})(1-\omega_{\perp})\nu_{21}E_{\perp} & 0 \\ (1-\omega_{\|})(1-\omega_{\perp})\nu_{12}E_{\|} & (1-\omega_{\perp})E_{\perp} & 0 \\ 0 & 0 & c(1-\omega_s)G \end{array} \right] \left\{ \begin{array}{c} \epsilon_{11} \\ \epsilon_{22} \\ \epsilon_{12} \end{array} \right\} \quad . \tag{3.4}$$

Following Eq. (2.3) the thermodynamic fluxes associated with the damage variables can be defined as

$$Y_{\|} = -\frac{\partial \Psi}{\partial \omega_{\|}} = \frac{E_{\|}}{2c^2} \left[\epsilon_{11} + (1-\omega_{\perp})\nu_{12}\epsilon_{22} \right]^2 \quad , \tag{3.5}$$

$$Y_{\perp} = -\frac{\partial \Psi}{\partial \omega_{\perp}} = \frac{E_{\perp}}{2c^2} \left[\epsilon_{22} + (1-\omega_{\|})\nu_{21}\epsilon_{11} \right]^2 \quad , \tag{3.6}$$

$$Y_s = -\frac{\partial \Psi}{\partial \omega_s} = 2G\epsilon_{12}^2 \quad . \tag{3.7}$$

The damage evolution criteria can now be represented in the space Y as a piecewise linear surface:

$$g_{\|} = 2\frac{E_{\|}}{X_{c,t}^2} Y_{\|} - r_{\|} = 0 \quad , \tag{3.8}$$

$$g_{\perp} = 2\frac{E_{\perp}}{Y_{c,t}^2} Y_{\|} + 2\frac{G}{S^2} Y_{12} - r_{\perp} = 0 \quad , \tag{3.9}$$

where symbols X, Y, and S denote the strengths in the direction parallel to the fibers, transverse to the fibers, and in-plane shear strength, respectively. The subscripts c, and t denote the values for compression and tension, respectively.

Neither the thermodynamic fluxes Y nor their rates are directly controllable in a loading process; therefore, it is reasonable to rewrite the damage criteria in Eqs. (3.5)–(3.7) and the damage loading conditions in Eqs. (3.8)–(3.9) by means of strain and strain rates:

$$g_{\|} = \frac{E_{\|}^2}{c^2 X_{c,t}^2} \left[\epsilon_{11} + (1-\omega_{\perp})\nu_{12}\epsilon_{22} \right]^2 - r_{\|}(\omega_{\|}) = 0 \quad . \tag{3.10}$$

$$g_{\perp} = \frac{E_{\perp}^2}{c^2 Y_{c,t}^2} \left\{ \left[\epsilon_{22} + (1-\omega_{\|})\nu_{21}\epsilon_{11} \right]^2 + \left[\frac{cGY_{c,t}}{E_{\perp}S} \epsilon_{12} \right]^2 \right\} - r_{\perp}(\omega_{\perp}) = 0 \quad . \tag{3.11}$$

To solve the loading ambiguity, the loading criteria have been introduced in the following

general form:

$$\hat{g} = \frac{\partial g}{\partial \epsilon} \cdot \dot{\epsilon} \quad , \tag{3.12}$$

which when applied to Eqs.(3.10) and (3.11) becomes:

$$\hat{g}_{\parallel} = \left[\epsilon_{11} + (1-\omega_{\perp})\nu_{12}\epsilon_{22}\right]\dot{\epsilon}_{11} + (1-\omega_{\perp})\nu_{12}\left[\epsilon_{11} + (1-\omega_{\perp})\nu_{12}\epsilon_{22}\right]\dot{\epsilon}_{22} \quad , \tag{3.13}$$

$$\begin{aligned} \hat{g}_{\perp} \quad = \quad & (1-\omega_{\parallel})\nu_{21}\left[\epsilon_{22} + (1-\omega_{\parallel})\nu_{21}\epsilon_{11}\right]\dot{\epsilon}_{11} \\ & + \left[\epsilon_{22} + (1-\omega_{\parallel})\nu_{21}\epsilon_{11}\right]\dot{\epsilon}_{22} + \left[\frac{2cGY_{c,t}}{E_{\perp}S}\right]^2 \epsilon_{12}\dot{\epsilon}_{12} \quad . \end{aligned} \tag{3.14}$$

The damage loading conditions can be expressed as

$$\begin{array}{cc} g = 0 \text{ and } \hat{g} > 0 & \text{loading} \\ g = 0 \text{ and } \hat{g} = 0 & \text{neutral loading} \\ g = 0 \text{ and } \hat{g} < 0 & \text{unloading} \\ g < 0 & \text{elastic} \end{array} \quad . \tag{3.15}$$

The damage evolution is based on Weibull distribution of defect strength, Reference 9. The details of damage mechanics implementation using this strength distribution can be found in Reference 10. The evolution law as a function of strain is given as

$$\omega = 1 - e^{-\frac{1}{me}\left(\frac{E\epsilon}{\sigma_{max}}\right)^m} \quad , \tag{3.16}$$

where m is the Weibull's exponent of strength distribution and σ_{max} is the ultimate strength of the composite. The methods for determining m from simple uniaxial tests are proposed in Reference 8. However, while the determination of the tensile parameter does show a physical relevance and applicability on a wide range of loadings and geometries, the compression behavior for composite tubes, especially in multi-ply configurations, cannot be directly related to the Weibull's parameter from the compressive coupon test since the respective deformation modes are significantly different. This shortcoming is characteristic of all the models presented in this report, and will be addressed in the future work by the development of an

interply cracking model for compression.

The combinations of Weibull's parameters and required material parameters for different loading situations are enumerated in Table 3.1.

	Parallel to fiber		Transverse to fiber		In-plane shear
	$\sigma_{11} \geq 0$	$\sigma_{11} < 0$	$\sigma_{22} \geq 0$	$\sigma_{22} < 0$	σ_{12}
ω	$\omega_{\parallel}$		$\omega_{\perp}$		ω_s
m	$m_{\parallel t}$	$m_{\parallel c}$	$m_{\perp t}$	$m_{\perp c}$	m_s
σ_{max}	X_t	X_c	Y_t	Y_c	S
ϵ	ϵ_{11}		ϵ_{22}		ϵ_{12}
E	$E_{\parallel}$		$E_{\perp}$		G

Table 3.1. Parameters for Eq. (3.16)

The strain rate effect in the material is modeled using viscous regularization of initially rate–independent damage formulation (see Eqs. (3.10), (3.11) and (3.16). In addition, viscous regularization alleviates problems associated with damage localization such as material softening and discretization sensitivity of the solution. The original formulation of the model in the Reference 5 uses nonsmooth damage surfaces. Therefore, some standard regularization techniques, such as viscous regularization of Perzyna's type[11] that was suggested in Reference 12, are not suited for this formulation. Instead, viscous regularization of the Duvant–Lions type[13] has been employed in this model because of its demonstrated advantages for application to nonsmooth damage surfaces. The rate–based constitutive equation is of the form

$$\dot{q} = -\tfrac{1}{\mu}\,(q - q^*) \quad \text{if} \quad g_\omega > 0 \quad , \tag{3.17}$$

where q denotes internal variables, q^* is the inviscid solution of rate-independent damage problem, g_ω is the the static damage surface, and μ is the viscosity coefficient. With the proper loading and unloading conditions, the generalized Duvant–Lions model renders a finite and unique solution even in the corner regions of a multifaceted damage surface. The formulation implemented in this model uses an implicit backward Euler algorithm. By

multiplying Eq. (3.17) by $\Delta t_n = (t_{n+1} - t_n)$ we obtain

$$\Delta q_{n+1} = -\frac{\Delta t_n}{\mu}\left(q_{n+1} - q^*_{n+1}\right) \quad , \tag{3.18}$$

where the subscript $n+1$ denotes the current time step. Solving for q_{n+1} yields

$$q_{n+1} = \frac{q_n + \Delta t_n/(\mu q^*_{n+1})}{1 + \Delta t_n/\mu} \quad , \tag{3.19}$$

where q_n is the damage variable solution from the previous step t_n. The internal variables used in the model are $\omega_\parallel$, $\omega_\perp$, ω_s, $r_\parallel$, and $r_\perp$ The associated stresses are obtained from Eq. (3.4). The limits of the instantaneous elasticity and inviscid damage response can be obtained by using very large and small values for μ, respectively. The integration algorithm proposed previously is unconditionally stable, which makes it suitable for both explicit and implicit time integration procedures.

4. HYDROSTATIC PRESSURE DEPENDENT DAMAGE MODEL

The basis for this model was developed from work documented in References 14–17. The damage is assumed to be produced by separate influences of deviatoric and hydrostatic stress components. This formulation models not only the damage–induced change in the elastic modulus of the material but also the respective variations of Poisson's ratio. According to this idea, the strain energy is divided into the deviatoric energy, Ψ_d, and the volumetric energy, Ψ_m, as

$$\Psi = \Psi_d + \Psi_m \quad . \tag{4.1}$$

In the state of plane stress, Eq. (4.1) becomes:

$$\Psi_d = (1-\omega_d)G(\epsilon' : \epsilon') = (1-\omega_d)G\left[\epsilon_{11}^2 + \epsilon_{22}^2 - \frac{\nu^2 - 4\nu + 1}{3(1-\nu^2)}(\epsilon_{11}+\epsilon_{22})^2 + 2\epsilon_{12}^2\right] \quad , \tag{4.2}$$

$$\Psi_m = (1-\omega_m)\frac{G(1+\nu)(1-2\nu)}{3(1-\nu^2)}(\epsilon_{11}+\epsilon_{22})^2 \quad , \tag{4.3}$$

where ϵ denotes the deviatoric part of the strain tensor. Following Equation (2.2), the stress relations are given as

$$\sigma_{11} = 2(1-\omega_d)G\left[\epsilon_{11} - \frac{\nu^2 - 4\nu + 1}{3(1-\nu^2)}(\epsilon_{11}+\epsilon_{22})\right] + 2(1-\omega_m)\frac{G(1+\nu)(1-2\nu)}{3(1-\nu^2)}(\epsilon_{11}+\epsilon_{22}) \quad , \tag{4.4}$$

$$\sigma_{22} = 2(1-\omega_d)G\left[\epsilon_{22} - \frac{\nu^2 - 4\nu + 1}{3(1-\nu^2)}(\epsilon_{11}+\epsilon_{22})\right] + 2(1-\omega_m)\frac{G(1+\nu)(1-2\nu)}{3(1-\nu^2)}(\epsilon_{11}+\epsilon_{22}) \quad , \tag{4.5}$$

$$\sigma_{12} = 2(1-\omega_d)G\epsilon_{12} \quad . \tag{4.6}$$

The associated damage fluxes are obtained using Eq. (2.3):

$$Y_d = G\left[\epsilon_{11}^2 + \epsilon_{22}^2 - \frac{\nu^2 - 4\nu + 1}{3(1-\nu^2)}(\epsilon_{11}+\epsilon_{22})^2 + 2\epsilon_{12}^2\right] \quad , \tag{4.7}$$

$$Y_m = \frac{G(1+\nu)(1-2\nu)}{3(1-\nu^2)}(\epsilon_{11}+\epsilon_{22})^2 \quad , \tag{4.8}$$

where ω_d and ω_m denote the deviatoric and hydrostatic damage variables, respectively. According to the second law of thermodynamics, the natural energy transfer is accompanied by an increase in entropy relative to the original state. In its mathematical form (Clasius-Duhem's inequality), this can be written as

$$\Phi = Y_d\dot{\omega}_d + Y_m\dot{\omega}_m - r\dot{\omega} \geq 0 \quad . \tag{4.9}$$

Inequality of Eq. (4.9) describes the energy dissipated through damage processes. It also implies that a damage surface exists as g_ω approaches zero. By introducing the Lagrangian multipliers into Eq. (4.9), it transforms into

$$\Phi = Y_d\dot{\omega}_d + Y_m\dot{\omega}_m - r\dot{\omega} - \lambda g_\omega \quad . \tag{4.10}$$

The inequality form of the 2nd law of thermodynamics now reduces to the problem of obtaining the extremum of the function in Equation 4.10, that is,

$$\begin{aligned}
\frac{\partial\Phi}{\partial Y_d} = 0 \quad &\Longrightarrow \quad \dot{\omega}_d = \dot{\lambda}\frac{\partial g_\omega}{\partial Y_d} \quad , \\
\frac{\partial\Phi}{\partial Y_m} = 0 \quad &\Longrightarrow \quad \dot{\omega}_m = \dot{\lambda}\frac{\partial g_\omega}{\partial Y_m} \quad , \\
\frac{\partial\Phi}{\partial r} = 0 \quad &\Longrightarrow \quad \dot{\omega} = \dot{\lambda}\frac{\partial g_\omega}{\partial r} \quad .
\end{aligned} \tag{4.11}$$

Ladaveze[18] proposed a damage criterion in the following form:

$$g_\omega = Y_d + \tau Y_m - r(\omega) \quad , \tag{4.12}$$

where

$$\tau = \frac{\omega_m}{\omega_d} \quad . \tag{4.13}$$

The preceeding equations do not express the unilateral character of the damage process. For most brittle materials, the tensile state induces significantly more damage in the material.

To account for such a behavior, the damage criterion can be modified as

$$g_\omega = Y_d + \langle \tau \rangle Y_m - r(\omega) \quad , \tag{4.14}$$

where the McAuley bracket is defined as

$$\langle \tau \rangle \quad = \quad \begin{cases} \tau & \text{if} \quad \sigma_m \geq 0 \\ 0 & \text{if} \quad \sigma_m < 0 \end{cases} \quad , \tag{4.15}$$

and σ_m is the hydrostatic stress. The physical meaning of Eq. (4.15) is that the negative hydrostatic stress does not contribute to damage evolution.

Using the notation similar to plastic flow relations, the damage evolution can be characterized as follows.

1. Damage evolution rule:

$$\begin{aligned} \dot{\omega}_d &= \dot{\lambda} \frac{\partial g_\omega}{\partial Y_d} = \dot{\lambda} \quad , \\ \dot{\omega}_m &= \dot{\lambda} \frac{\partial g_\omega}{\partial Y_m} = \langle \tau \rangle \dot{\lambda} \quad . \end{aligned} \tag{4.16}$$

2. Damage hardening rule:

$$\begin{aligned} \dot{\omega} &= \dot{\lambda} \frac{\partial g_\omega}{\partial r} = \dot{\lambda} \quad , \\ \dot{r} &= \frac{dr}{\partial \omega} = \frac{dr}{\partial \omega} \dot{\lambda} \quad . \end{aligned} \tag{4.17}$$

3. Damage loading and unloading rule:

$$g_\omega \leq 0 \quad , \quad \dot{\lambda} \geq 0 \quad , \quad \dot{\lambda} g_\omega = 0 \quad . \tag{4.18}$$

Conditions in Eq. (4.18) are expressed in the standard Kuhn-Tucker form and describe the unilateral character of the damage evolution. If $g_\omega < 0$, then the damage criterion in Eq. (4.18) implies that $\dot{\lambda} = 0$; hence, the damage evolution rule in Eq. (4.15) implies that

$\omega_d = \omega_m = 0$, and no further damage is incured. If $\lambda > 0$, that is, if further damage occurs, the condition in Eq. (4.18) implies that $g_\omega = 0$. Therefore, the damage surface separates the damaged from the undamaged state. Since the damage surface is smooth, the damage viscous regularization of Perzyna's type can be used. The particular structure of the regularization proposed in Reference 11 has been used in the model. The rate equations governing linear viscous-damage behavior are obtained from the rate-independent form by replacing r by $\dot{r}$. The regularization of the damage variables can be then written as

$$\dot{r} = \frac{\langle g_\omega \rangle}{\mu} \quad , \tag{4.19}$$

$$\dot{\omega}_d = \frac{d\omega}{dr}\dot{r} \quad , \tag{4.20}$$

$$\dot{\omega}_m = \langle \tau \rangle \dot{\omega}_d \quad . \tag{4.21}$$

Thus, if the damage takes place,

$$g_\omega = Y_{d,n+1} + \langle \tau \rangle Y_{m,n+1} - r_n > 0 \quad . \tag{4.22}$$

Applying the implicit backward Euler algorithm from Eqs. (3.17)–(3.19) to Eq. (4.21) yields

$$r_{n+1} = r_n + \frac{\Delta t_n}{\mu} g_{\omega,n+1} = r_n + \frac{\Delta t_n}{\mu} \left(Y_{d,n+1} + \langle \tau \rangle Y_{m,n+1} - r_{n+1} \right) \quad . \tag{4.23}$$

Finally, the rate form of the damage evolution is

$$r_{n+1} = \frac{r_n + \Delta t_n/\mu \left(Y_{d,n+1} + \langle \tau \rangle Y_{m,n+1} \right)}{1 + \Delta t_n/\mu} \quad , \tag{4.24}$$

$$\omega_{d,n+1} = \omega_{d,n} + \frac{d\omega}{dr}(r_{n+1} - r_n) \quad , \tag{4.25}$$

$$\omega_{m,n+1} = \omega_{m,n} + \langle \tau \rangle (\omega_{d,n+1} - \omega_{d,n}) \quad . \tag{4.26}$$

Equation 4.26 has two indications: (1) as $\mu \to \infty$, $r_{n+1} \to r_n$; thus, $\omega_{d,n+1} \to \omega_{d,n}$, and $\omega_{m,n+1} \to \omega_{m,n}$. Hence, no further damage occurs during the increment, and the instantaneous elastic response is recovered. (2) As $\mu \to 0$, $r_{n+1} \to Y_{d,n+1} + \langle \tau \rangle Y_{m,n+1}$, which results in the rate-independent damage formulation. This shows the properly bounded behavior for

the two extreme cases with a smooth transition in between.

The model presented here is based on positive hydrostatic pressure–dependent damage evolution. For composite materials, both positive and negative hydrostatic pressure may contribute to damage. This characteristic has been accounted for in the present model by replacing the McAuley bracket in Eq. (4.14) with

$$\langle \tau \rangle \quad = \quad \begin{cases} \tau_+ & \text{if} \quad \sigma_m \geq 0 \\ \tau_- & \text{if} \quad \sigma_m < 0 \end{cases} \quad . \tag{4.27}$$

The magnitude of τ_+ is generally larger than τ_- for most materials.

5. DAMAGE MODEL WITH STRAIN TENSOR SPLIT

The previous two damage models were implemented into DYNA3D[19] code and were used for simulations of the CSM composite tube drop-tower tests. Although the two models have shown encouraging results, in general they have not yielded a satisfactory modeling approach that would easily be applicable to a large span of CSM composite tube geometries and loading configurations. The deficiencies of these formulations for modeling of the CSM composites have been analyzed, and directions for further model developments have been identified. As a result of this effort, a new model based on separation of the compression and tension effects on damage development in CSM composite materials has been developed. The concept of the separation of the strain tensor is used to account for two basic tensile and compressive damage evolution processes. This idea was motivated by work in References 20 and 21. The justification for the new model based on the experimental observations in tube impact tests and theoretical developments are presented in Reference 2.

The formulation of the model starts from the separation of the strain energy into tension and compression parts as

$$\Psi = (1-\omega_+)G\left[(\epsilon^+ : \epsilon^+) + \frac{4\nu}{1-\nu}(\epsilon_m^+)^2\right] + (1-\omega_-)G\left[(\epsilon^- : \epsilon^-) + \frac{4\nu}{1-\nu}(\epsilon_m^-)^2\right] \quad , \qquad (5.1)$$

where ϵ^+ and ϵ^- denote the positive and the negative part of the strain tensor, respectively. Variables ω_+ and ω_- denote the associated tensile and compression damage variables, respectively. The positive part of the strain tensor is obtained by using a positive projection operator P^+, which removes contributions of negative eigenvalues of the strain tensor:

$$\epsilon^+ = P^+ \cdot \epsilon \quad . \qquad (5.2)$$

The negative part of the strain tensor is then

$$\epsilon^- = P^- \cdot \epsilon \quad . \qquad (5.3)$$

The projection operators satisfy the following relations:

$$\epsilon^- = \epsilon - \epsilon^+ \quad , \tag{5.4}$$

$$P^- = I - P^+ \quad . \tag{5.5}$$

where I denotes the fourth-order identity tensor and P^+ and P^- are symmetric. The projection operator can be written as

$$P^+_{ijkl} = \frac{1}{2}\left(S^+_{ik}S^+_{jl} + S^+_{il}S^+_{jk}\right) \quad . \tag{5.6}$$

The symmetric matrix S^{20} is defined as

$$S^+ = \sum_{i=1}^{3} \langle \epsilon_i \rangle |\epsilon_i| n_i \otimes n_i \quad , \quad |n_i| = 1 \quad , \tag{5.7}$$

where ϵ_i is the principal strains and n_i denotes the corresponding principal directions. The $\langle\rangle$ symbol denotes the Heaviside step function that is used to remove the contributions of the negative strain tensor eigenvalues:

$$\langle x \rangle = \begin{cases} 1 & \text{if} \quad x \geq 0 \\ 0 & \text{if} \quad x < 0 \end{cases} \quad . \tag{5.8}$$

If we now proceed using the Eq. (2.2) in the introductory part of the report, we obtain stress relations as

$$\sigma_{11} = \frac{2(1-\omega_+)G}{1-\nu}\left[\epsilon^+_{11} + \nu\epsilon^+_{22}\right] + \frac{2(1-\omega_-)G}{1-\nu}\left[\epsilon^-_{11} + \nu\epsilon^-_{22}\right] \quad , \tag{5.9}$$

$$\sigma_{22} = \frac{2(1-\omega_+)G}{1-\nu}\left[\epsilon^+_{22} + \nu\epsilon^+_{11}\right] + \frac{2(1-\omega_-)G}{1-\nu}\left[\epsilon^-_{22} + \nu\epsilon^-_{11}\right] \quad , \tag{5.10}$$

$$\sigma_{12} = 2(1-\omega_+)G\epsilon^+_{12} + 2(1-\omega_-)G\epsilon^-_{12} \quad , \tag{5.11}$$

the associated damage forces using Eq. (2.3) are

$$Y_+ = G\left[(\epsilon^+ : \epsilon^+) + \frac{4\nu}{1-\nu}(\epsilon^+_m)^2\right] \quad , \tag{5.12}$$

$$Y_- = G\left[(\epsilon^- : \epsilon^-) + \frac{4\nu}{1-\nu}(\epsilon_m^-)^2\right] \quad . \tag{5.13}$$

By adopting a damage criterion for each of associate damage variables, damage surfaces become

$$g_+ = \frac{4G(1-\nu)}{X_+^2}Y_+ - r_+ = \left(\frac{2G}{X_+}\right)^2\left[(1-\nu)\epsilon^+ : \epsilon^+ + 4\nu(\epsilon_m^+)^2\right] - r_+ \quad , \tag{5.14}$$

$$g_- = \frac{4G(1-\nu)}{X_-^2}Y_- - r_- = \left(\frac{2G}{X_-}\right)^2\left[(1-\nu)\epsilon^- : \epsilon^- + 4\nu(\epsilon_m^-)^2\right] - r_- \quad , \tag{5.15}$$

where X_+ and X_- are the tensile and the compressive strengths, respectively, and r_+ and r_- are the associated damage thresholds. The damage loading criteria can then be written as

$$\hat{g}_+ = \left[\epsilon_{11}^+ + \nu\langle\epsilon_1\rangle\langle\epsilon_2\rangle\epsilon_{22}^+\right]\dot{\epsilon}_{11} + \left[\epsilon_{22}^+ + \nu\langle\epsilon_1\rangle\langle\epsilon_2\rangle\epsilon_{11}^+\right]\dot{\epsilon}_{22} + 2(1-\nu)\epsilon_{12}^+\dot{\epsilon}_{12} \quad , \tag{5.16}$$

$$\hat{g}_- = \left[\epsilon_{11}^- + \nu\langle-\epsilon_1\rangle\langle-\epsilon_2\rangle\epsilon_{22}^-\right]\dot{\epsilon}_{11} + \left[\epsilon_{22}^- + \nu\langle-\epsilon_1\rangle\langle-\epsilon_2\rangle\epsilon_{11}^-\right]\dot{\epsilon}_{22} + 2(1-\nu)\epsilon_{12}^-\dot{\epsilon}_{12} \quad . \tag{5.17}$$

The evolution of damage variables is governed by the same expressions as for the anisotropic model, that is,

$$\omega = 1 - e^{-\frac{1}{m_+ e}\left(\frac{2G\epsilon^+}{(1-\nu)X_+}\right)^{m_+}} \quad , \tag{5.18}$$

$$\omega = 1 - e^{-\frac{1}{m_- e}\left(\frac{2G\epsilon^-}{(1-\nu)X_-}\right)^{m_-}} \quad , \tag{5.19}$$

where

$$\epsilon^+ = (1-\nu)\epsilon^+ : \epsilon^+ + 4\nu(\epsilon_m^+)^2 \quad , \tag{5.20}$$

$$\epsilon^- = (1-\nu)\epsilon^- : \epsilon^- + 4\nu(\epsilon_m^-)^2 \quad . \tag{5.21}$$

A viscous regularization of damage variables analogous to the one for the anisotropic damage model in Eqs. (3.17) through (3.19) has been used to model the rate dependency of the material.

6. CRUSH FRONT MODEL

Crush front model was first introduced in work by Hallquist and Matzenmiller in Reference 5. Although it is difficult to state all the reasons the authors had for introducing the crush front, one reason seemed to be a reduction of force that was transmitted along the length of the tube. If the strength of the elements adjacent to the impact region were not reduced, the forces could be carried high up the tube where they could induce a catastrophic failure.

Although at first glance the crush front concept seems to be a numerical gimmick to obtain a progressive crush, it compensates for structural and material mechanisms that are present in tube crush. The recent tube studies by ORNL and the Automotive Composites Consortium (ACC) have shown that the impact zone experiences significant delamination both between plies (braid) and within plies (CSM). The interply cracks are propagating ahead of the impact zone and reducing the strength and rigidity of the composite through instability mechanisms. The compressive strength of a set of delaminated plies is vastly reduced compared to the uncracked laminate. The iterply cracking effectively reduces the strength of the material adjacent to the crush zone and provides for a stable, progressive crush. Therefore, although originally introduced mostly for numerical reasons, the crush front model can also be used as a mathematical model for progressive tube crush.

An apparent question is how to identify and quantify the crush front model's parameters. That question, and the concerns about lumping all the underlying out-of-plane deformation mechanisms into a single model has caused authors to stop further development on the crush front, and to incorporate modeling of interply cracking during tube compression into the constitutive model of material.

In the Hallquist and Matzenmiller model, a new element is enrolled into a crush front if it shares nodes with a failed element, where an element is considered to be failed if its characteristic time step falls below the specifed value. Our implementation has two new improvements:

1. The elements are considered failed if the amount of internal damage reaches maximum value. This approach is more physically justified and can prevent excessive element

deformations that are present in Reference 5.

2. Nodes have indicators that count the number of failed elements connected to them. The node information is then used to determine the intensity and propagation of reduction of material properties ahead of failed elements. This enables a faster crush front propagation for regions with geometric features that favor crush propagation (e.g., corners). Figure 1 illustrates the concept of weighted crush front propagation where a higher number indicates a larger strength reduction.

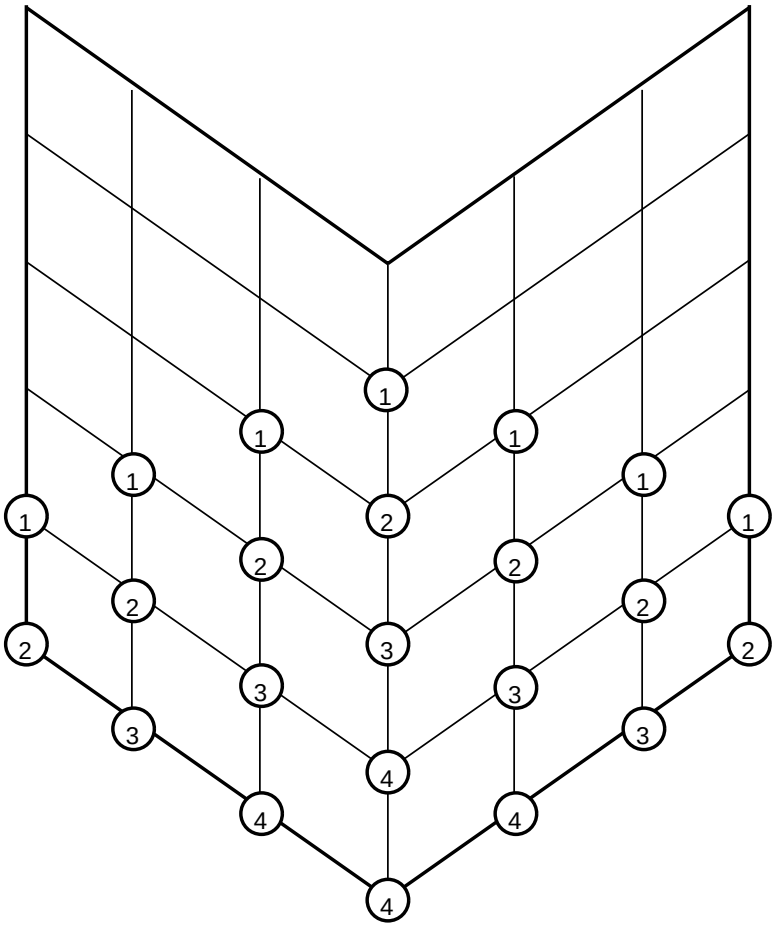

Figure 1. Weighted crush front propagation

7. NUMERICAL RESULTS

The developed models were implemented in the finite element program DYNA3D and used for simulation of drop tower tests of tubular CSM components. The tests were perfomed by ACC and were provided for comparison with simulation models. A typical configuration of the drop tower test is shown in Fig. 2 The test specimen is fixed on the drop tower beam and raised to the predetermined height. The beam is then released, and the specimen impacts the impact plate that is instrumented with a force measurement sensor. The resulting deformed CSM specimen from ACC test number 4041 is shown in Fig. 3.

7.1. Damage Model for Unidirectional Fiber Composites

This model was primarily used as a benchmark to evaluate the capabilities that were considered as state-of-the-art in the current literature. The model was used for simulation of tube impact where it was assumed that the tube was composed on multiple plies of fiber aligned in either the longitudinal or the hoop direction of the tube. The ACC has not performed tests with such a tube, and the results presented here are for illustration of the tendencies of the model behavior. The sequence of deformed shapes for a tube with fibers aligned in the longitudinal and the hoop directions of the tube is shown in Figs. 4 – 5 and 6 – 7, respectively. In the case when the fibers are aligned in the longitudinal direction of the tube the corner cracks propagate well ahead of the impact zone thus changing the tube impact into the impact of four separate fronds. In the case of hoop-aligned fibers, the tube still deforms into four separate fronds but with very short corner crack advancement. The resulting force on the impactor plate for both longitudinal and hoop alignments of the fibers is shown in Fig. 8. This model has a very stable behavior without the crush front model. Previous commercial implementation of this model required the crush-front model to stabilize tube deformation and, therefore, introduced an additional parameter that could not be easily determined from experiments.

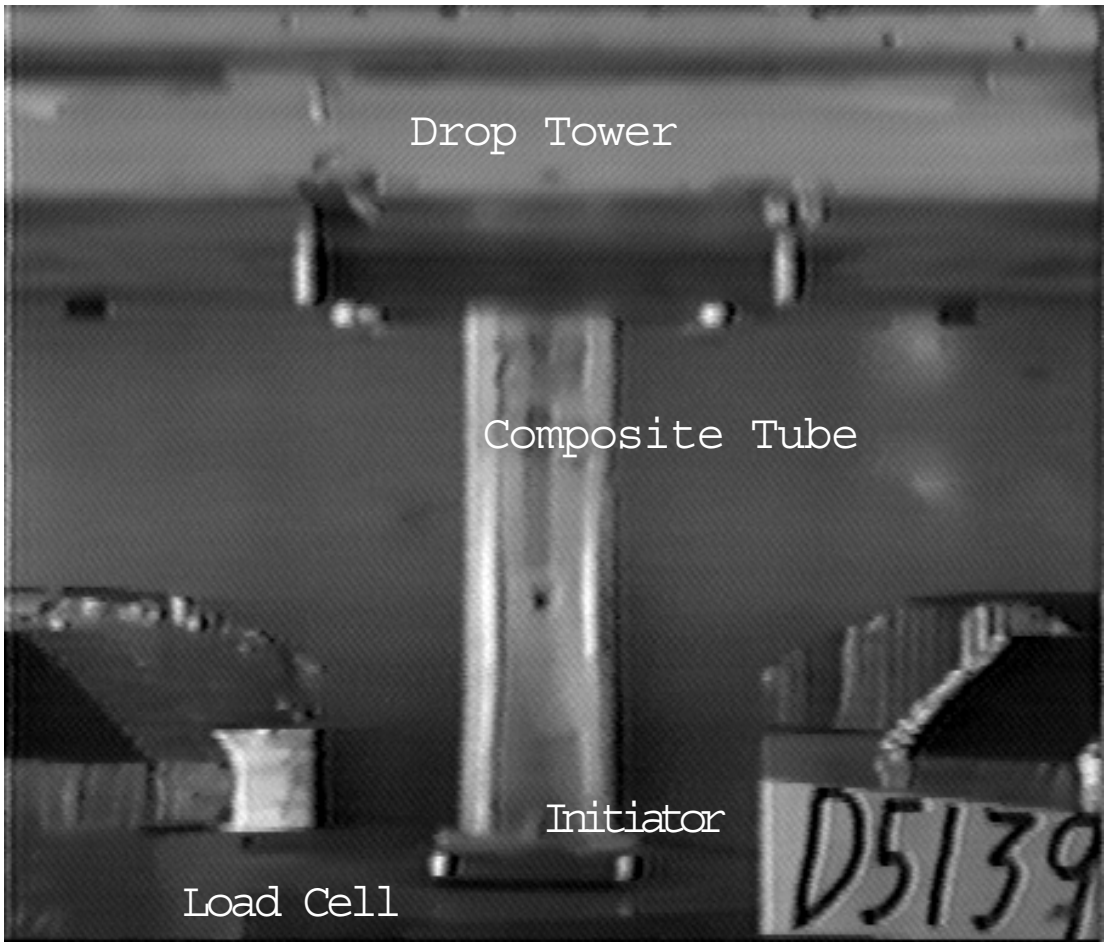

Figure 2. Drop Tower Test Configuration

Figure 3. Deformed CSM Specimen after Drop Tower Test

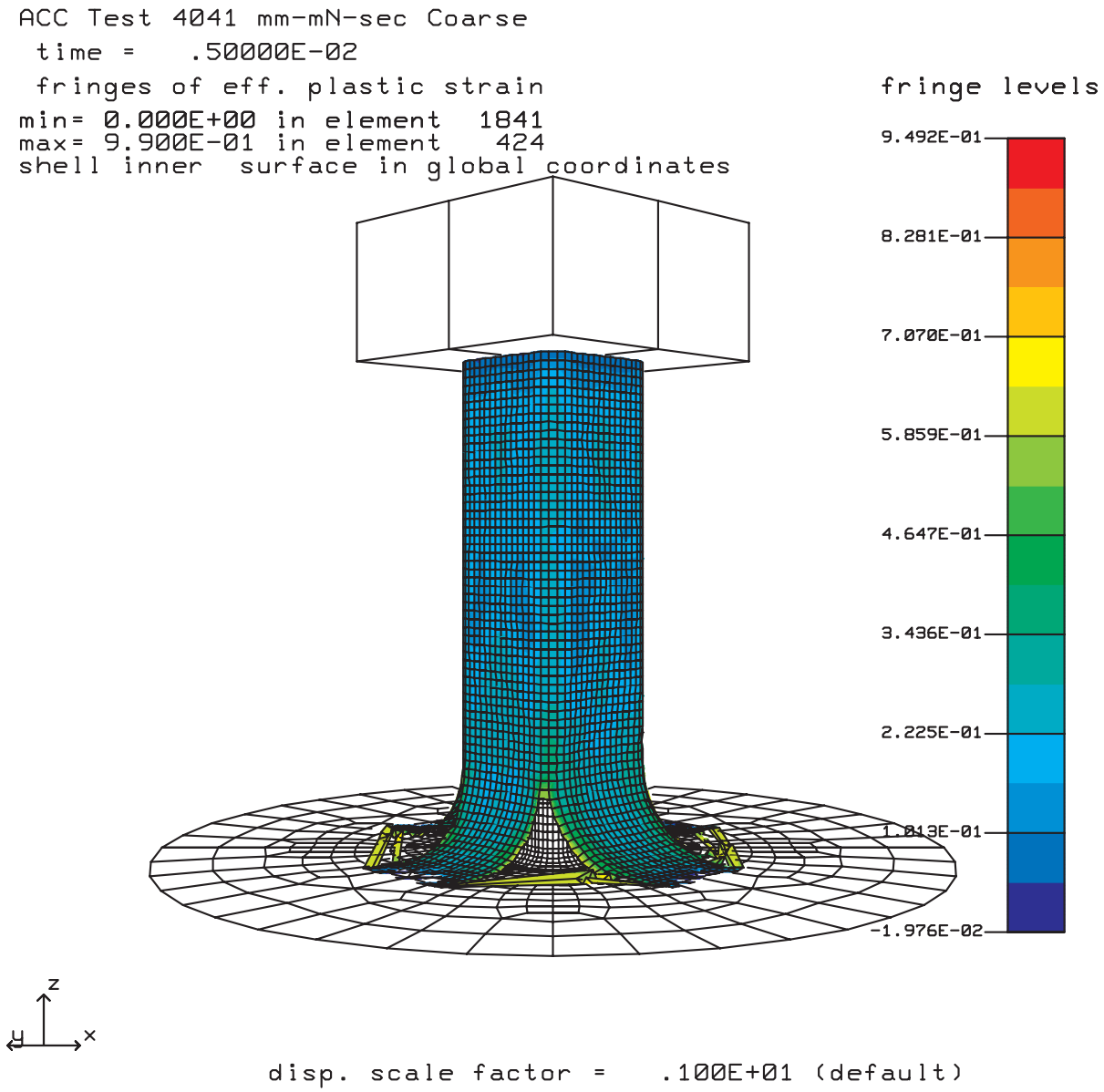

Figure 4. Material 52, Tube Deformation, 0^o Fibers

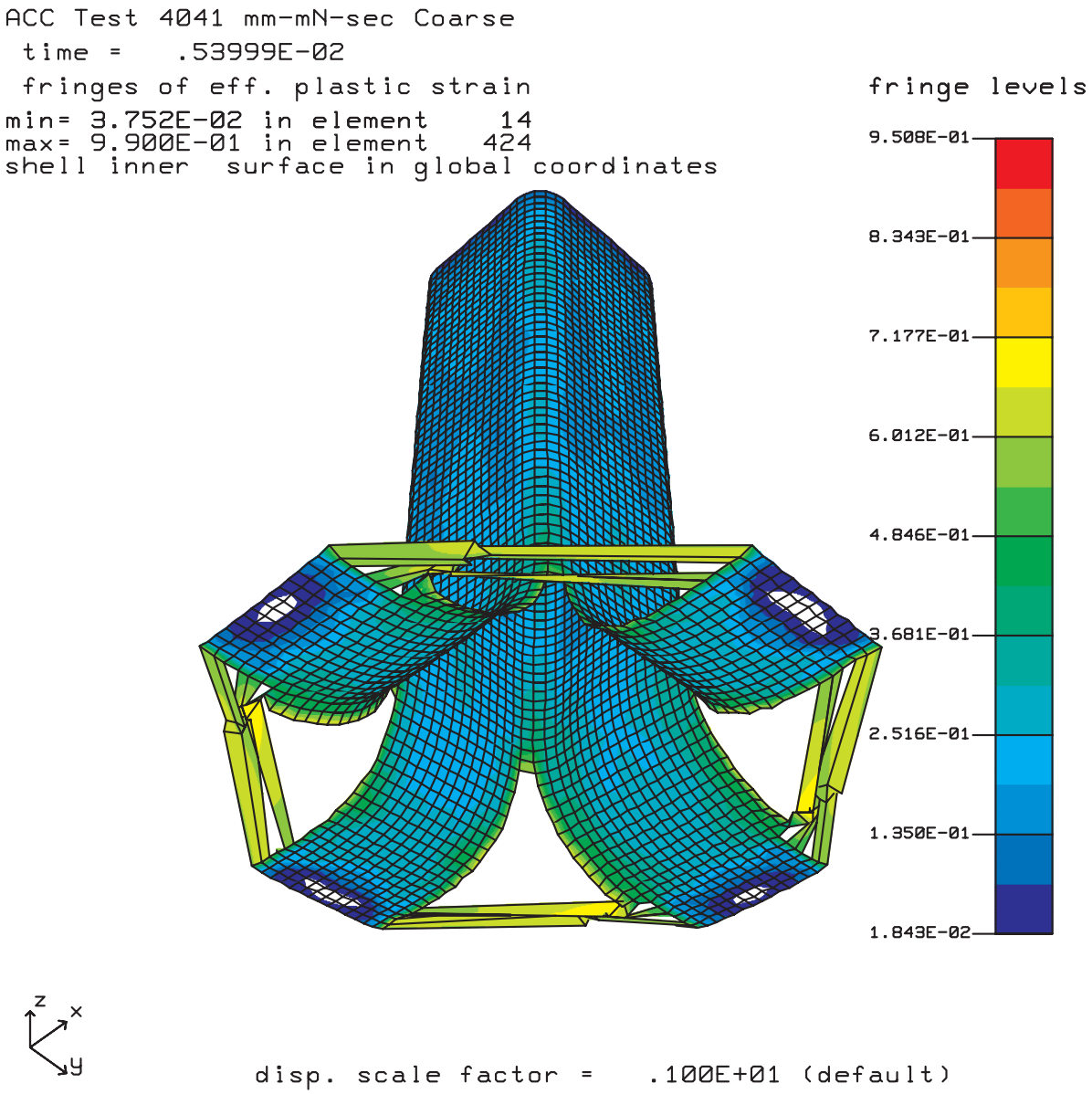

Figure 5. Material 52, Tube Deformation, 0^o Fibers

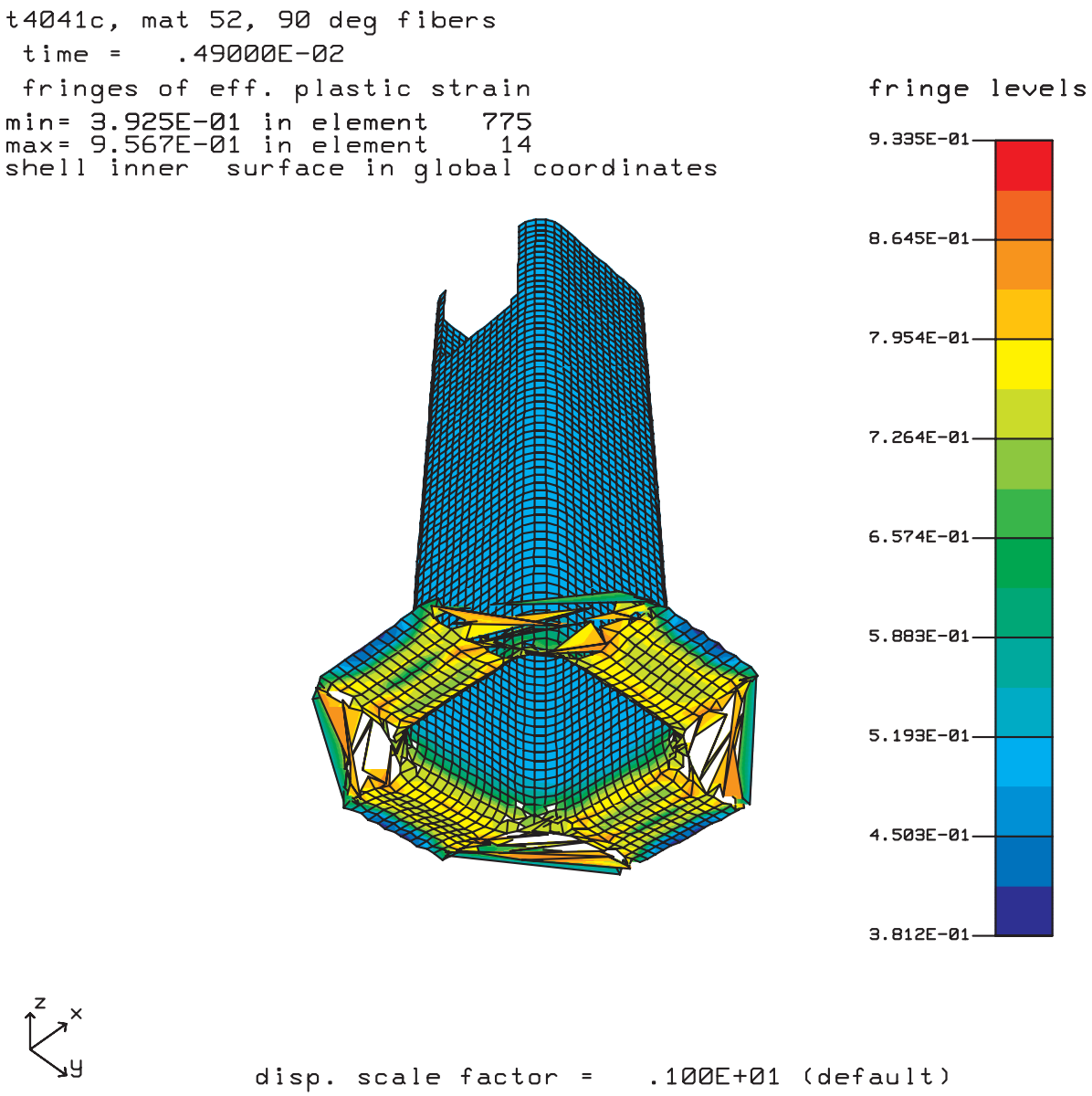

Figure 6. Material 52, Tube Deformation, 90^o Fibers

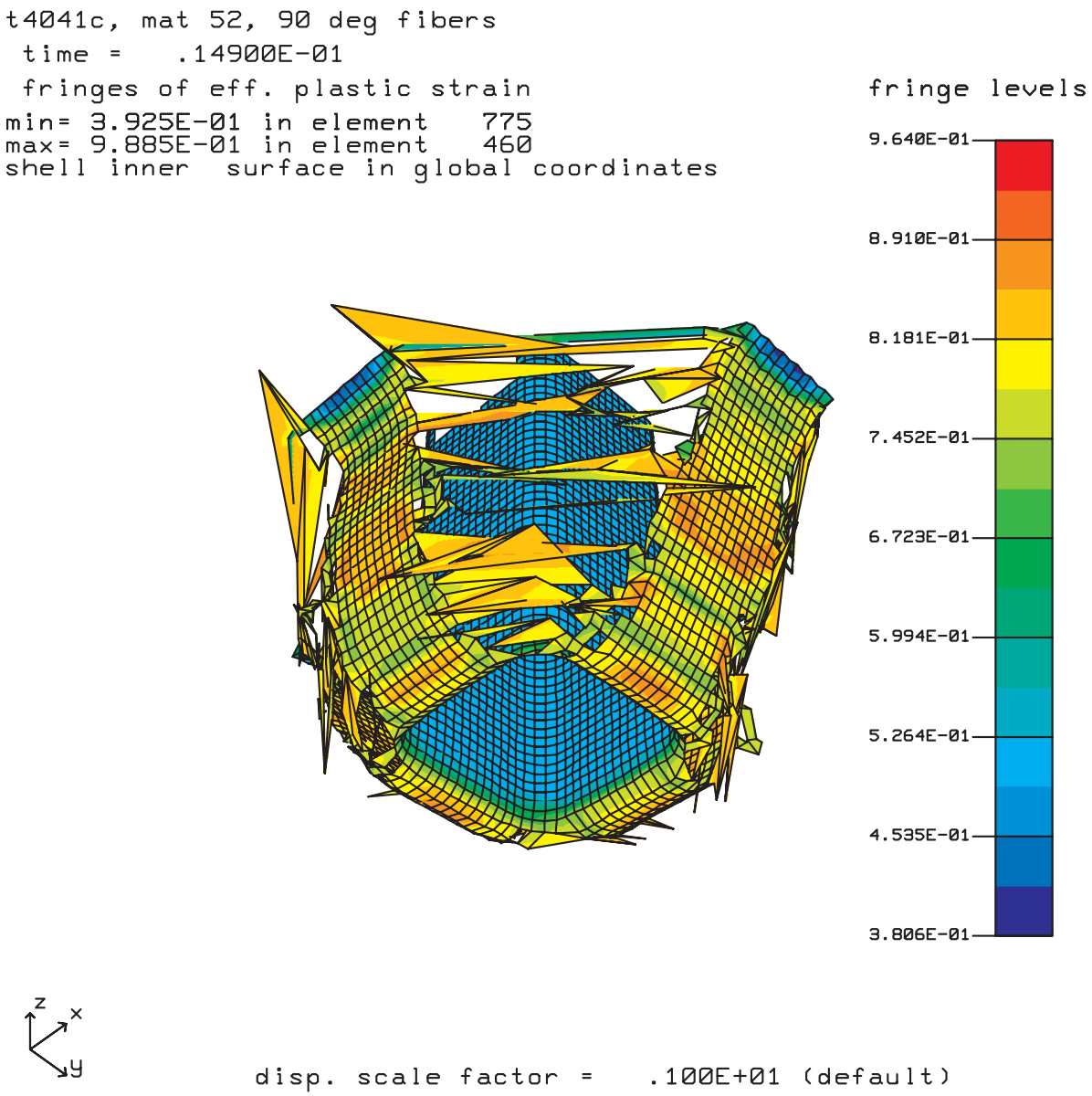

Figure 7. Material 52, Tube Deformation, 90^o Fibers

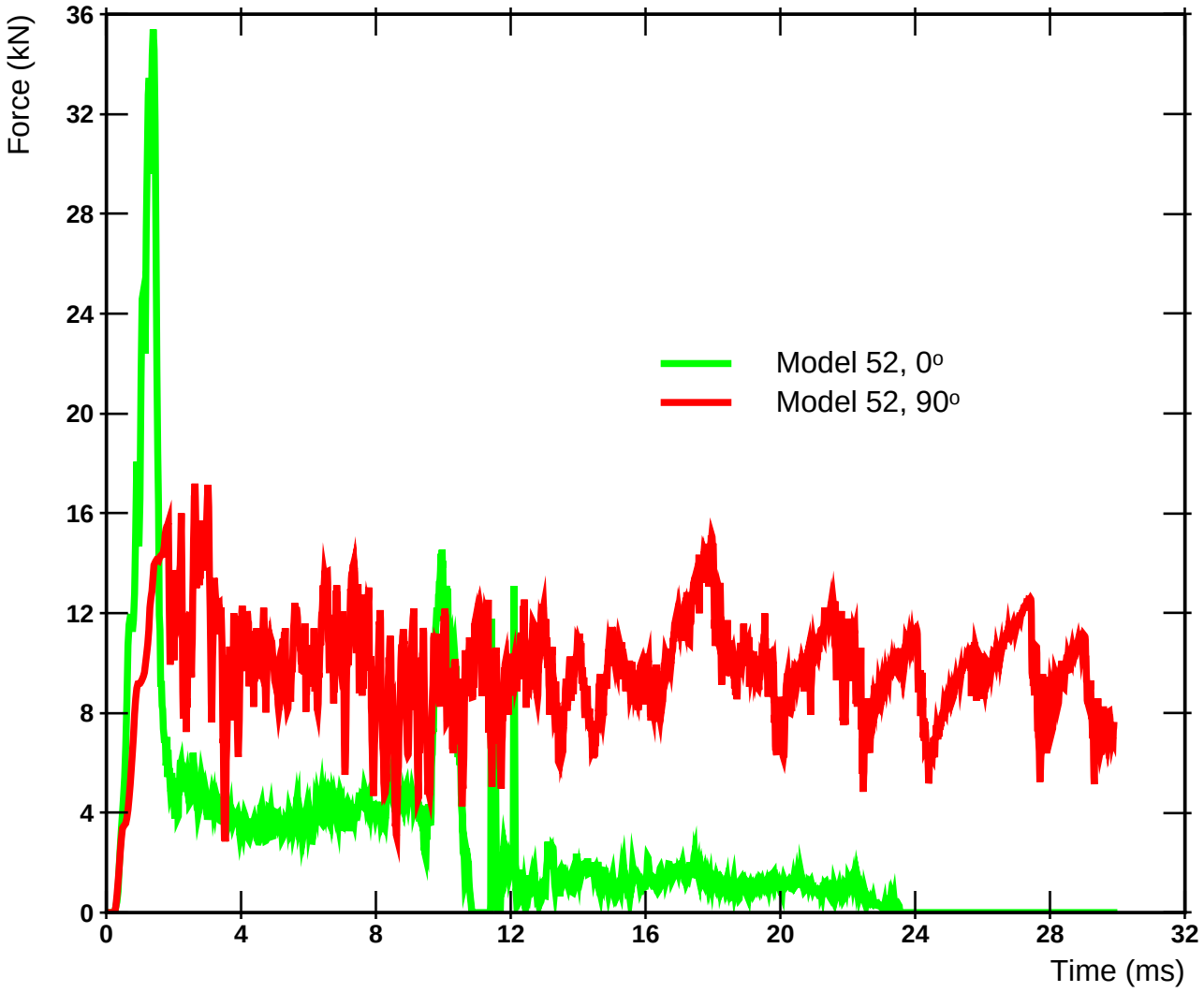

Figure 8. Material 5, Barrier Force

7.2. Hydrostatic Pressure–Dependent Damage Model

The hydrostatic pressure–dependent damage model was designed to model the deformation in CSM tubes by modeling separate influences of the hydrostatic and deviatoric parts of the stress tensor. All of the model's parameters were to be determed from experiments. The lack of experimental data neccessary for model definition and problems with measurement of damage evolution with increased loading are the main reasons why the model did not yield suitable results. The material properties for this model were derived from DELSEN experiments[22, 23] and are included in Chap. 8. However, the tests were not instrumented to the degree that would provide enough information for the necessary model parameters and, therefore, many of the damage evolution related parameters had to be assumed. The sequence of deformed geometries for tube impact is shown in Figs. 9 – 10. The resulting force on the impactor plate for failure damage of $\omega_{max} = 0.6$ and $\omega_{max} = 0.9$, respectively, is shown in Fig. 11. The force levels from the simulations are much lower than for the experiment. Modification of model parameters could substantially improve the results, however, it was decided not to pursue the development of this model, primarily because of the sophisticated instrumentation necessary for proper experimental characterization.

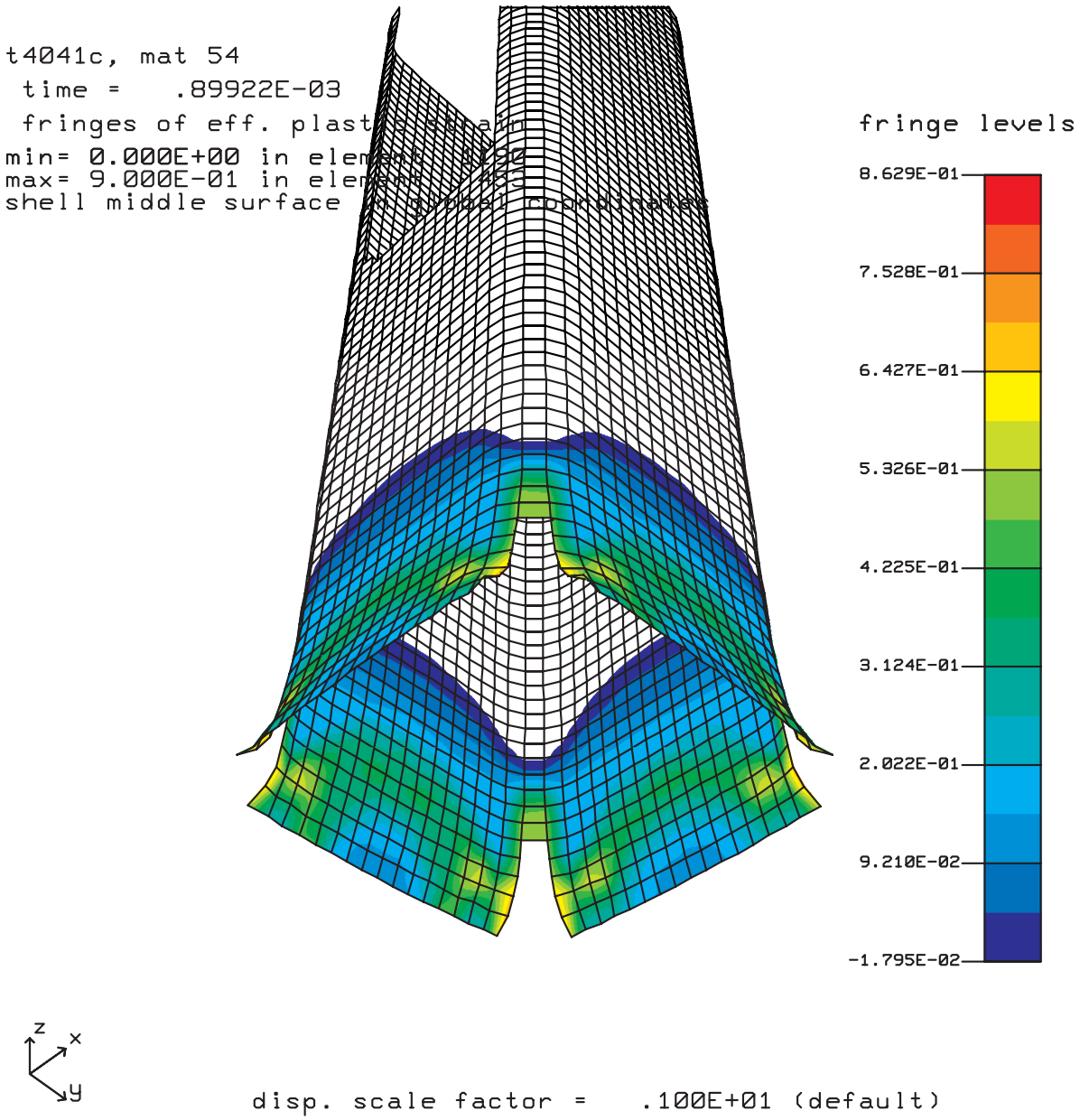

Figure 9. Material 54, Tube Deformation 1

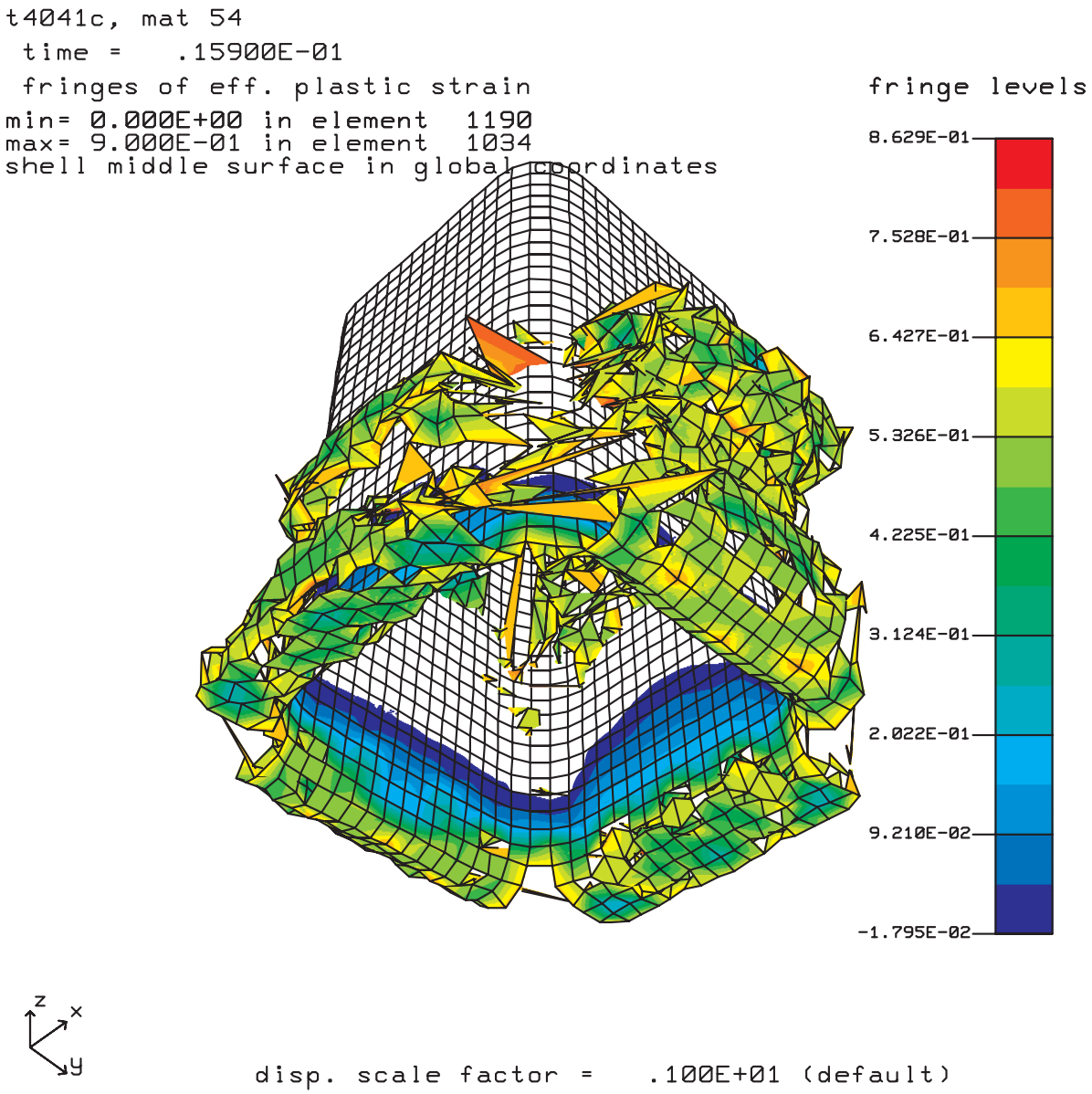

Figure 10. Material 54, Tube Deformation 2

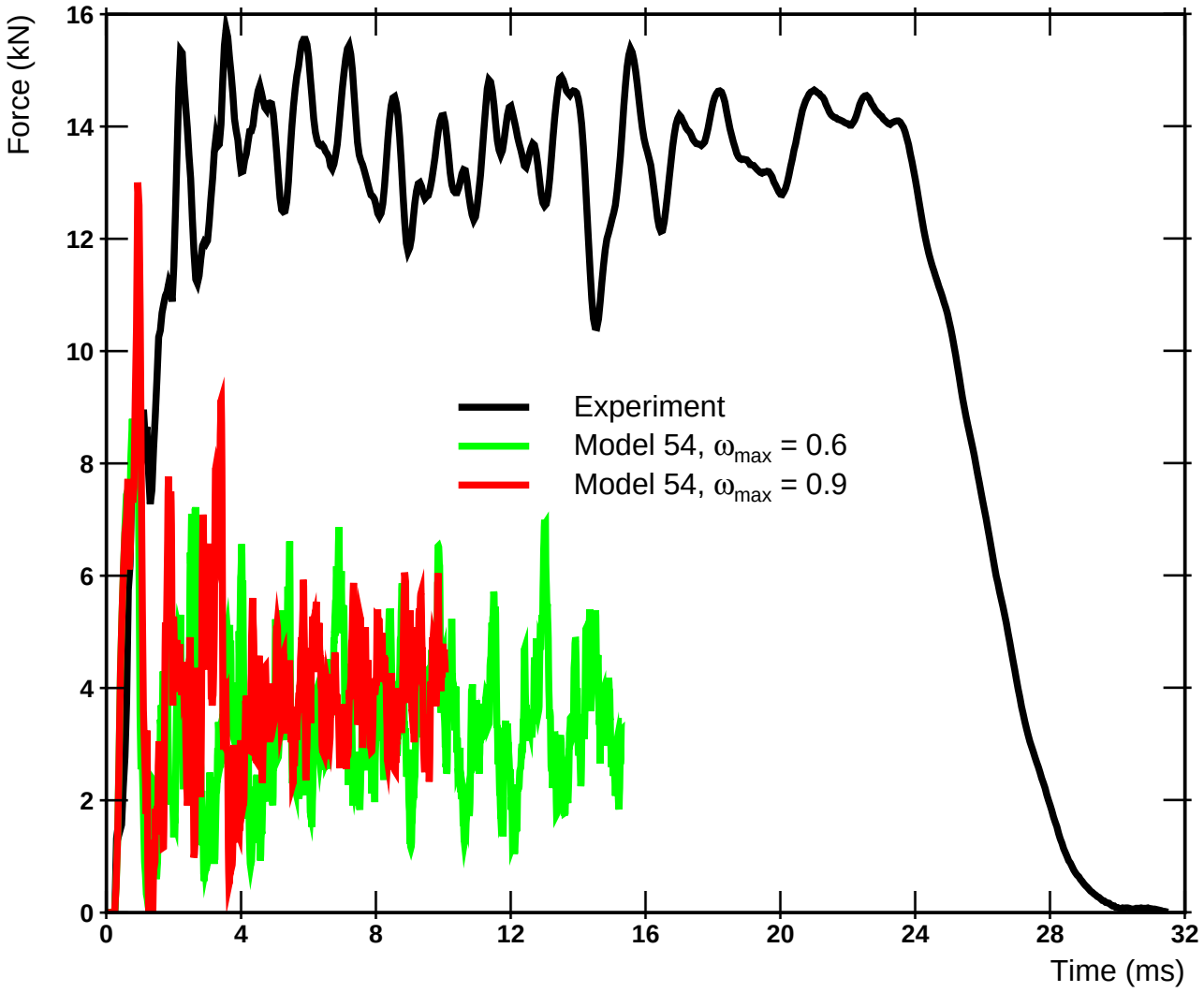

Figure 11. Material 54, Barrier Force

7.3. Damage Model with Strain Tensor Split

The damage model with strain tensor split draws from the successful ideas of the anisotropic and hydrostatic models. It combines the assumed flaw distribution from the anisotropic model and energy separation from the hydrostatic model. The results obtained using this model have shown very good agreement with experimental data for different tube geometries. However, determining the values for the strength distribution coefficients m_+ and m_- requires some additional comments.

The model splits the deformation into the tensile and the compressive parts. In tension mode it is reasonable to assume that the material behaves similarly to the coupon test (for an in-depth discussion of the physical deformation mechanisms in the CSM composites see Reference 2. Therefore, the range of the tensile m_+ coefficient is typically in the range of 2 to 4, depending on the value that best approximates tensile coupon stress-strain curve. Figure 12 illustrates determination of the m_+ coefficient based on experimentally measured elastic modulus and strength of the CSM composite coupon. Measured values are taken from the coupon test for the material used in tube test 4041.

In the compression mode, however, several concurrent mechanisms reduce the stiffness of the material (longitudinal intraply and interply cracking, and instability–driven delamination) and are associated with out-of-plane stresses that cannot be effectively modeled using the Belytscko-Tsay shell. The average compressive deformation of tube fronds is well above the values obtained from compressive coupon tests. The developed model can compensate for these effects by reducing the magnitude of the compresison strength parameter m_- to a value is typically in the range of 1 to 2. This reduction can also be estimated by assuming delamination between the plies that is in the range of ply thickness. The exact value is difficult to determine since, after all, it is only a crude approximation of the effects arising from multiple out-of-plane deformation modes by in-plane effects and experimental results show significant scatter. Lower values of m_- result in a more compression–compliant material that can sustain larger deformation compared to high m_- values. To keep the allowed deformation in a realistic range, the total deformation in a finite element was limited by the maximum amount of total damage in both modes after which the element was removed from calculation.

Simulated progression of the tube impact for drop tower test 4041 using relatively coarse finite element discretization is shown in Figs. 13 – 16. The view from the impactor plate shows tearing along the tube corners and continuous inversion of the fronds. To evaluate the discretization dependency of the model, a much finer finite element mesh was employed. Simulation results using the fine element mesh are shown in Figs. 17 – 18. The resulting force traces on the impactor plate for both discretizations are shown in Fig. 19. A very good agreement between the simulation and the experiment for both finite element discretizations can be observed.

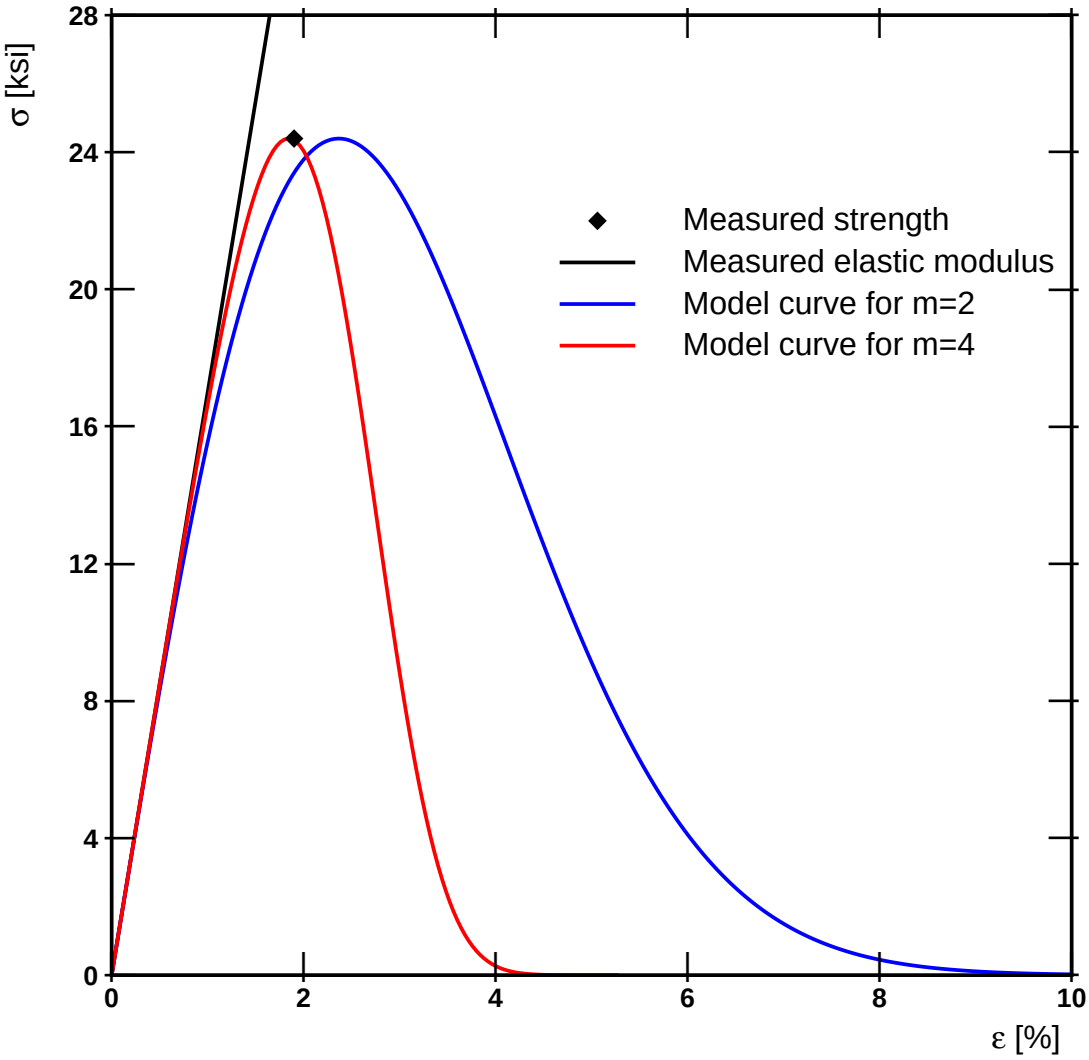

Figure 12. Material 53, Determination of m Value from Experiments

Figure 13. Material 53, Coarse Mesh

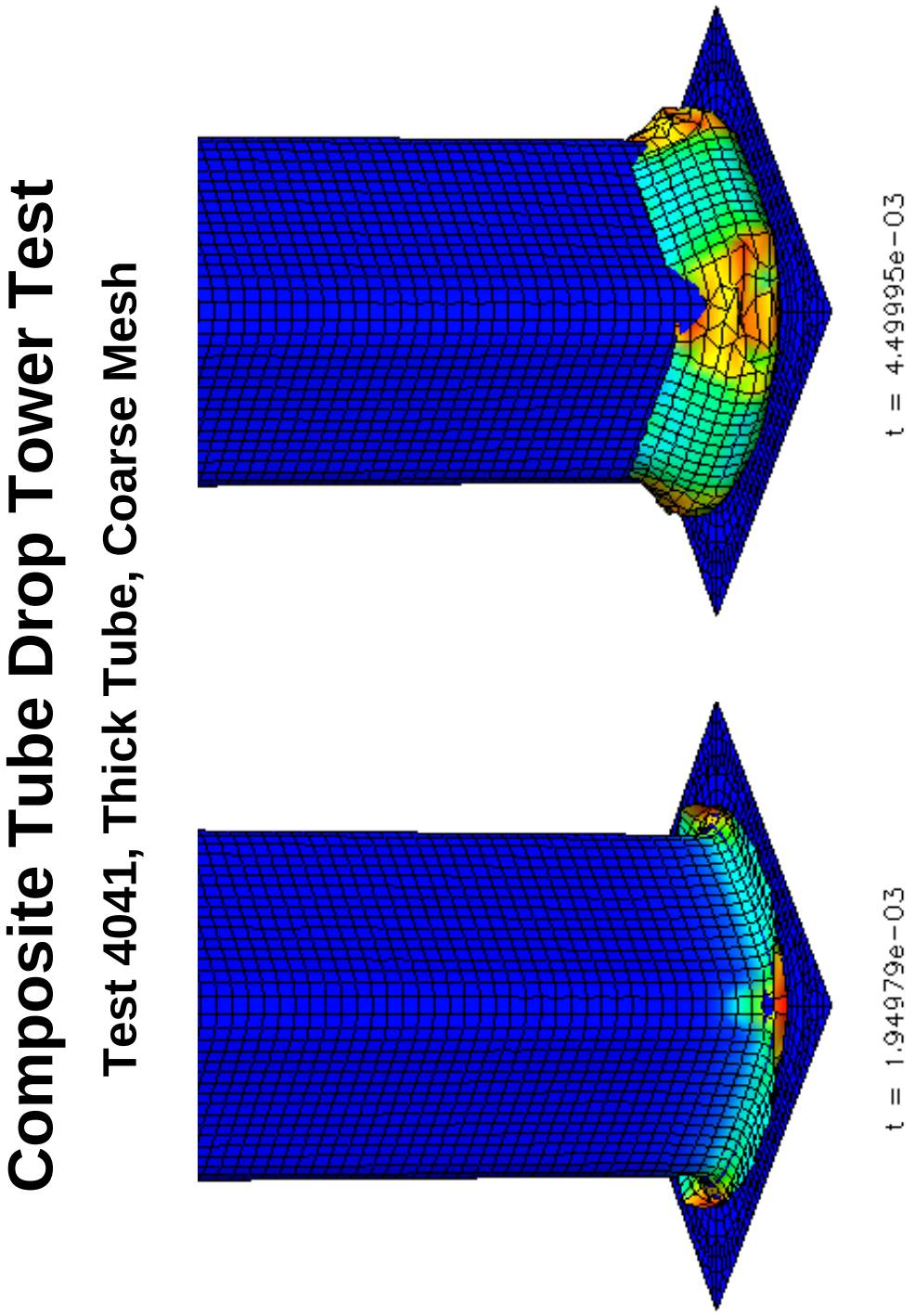

Figure 14. Material 53, Coarse Mesh, Deformation Sequence 1

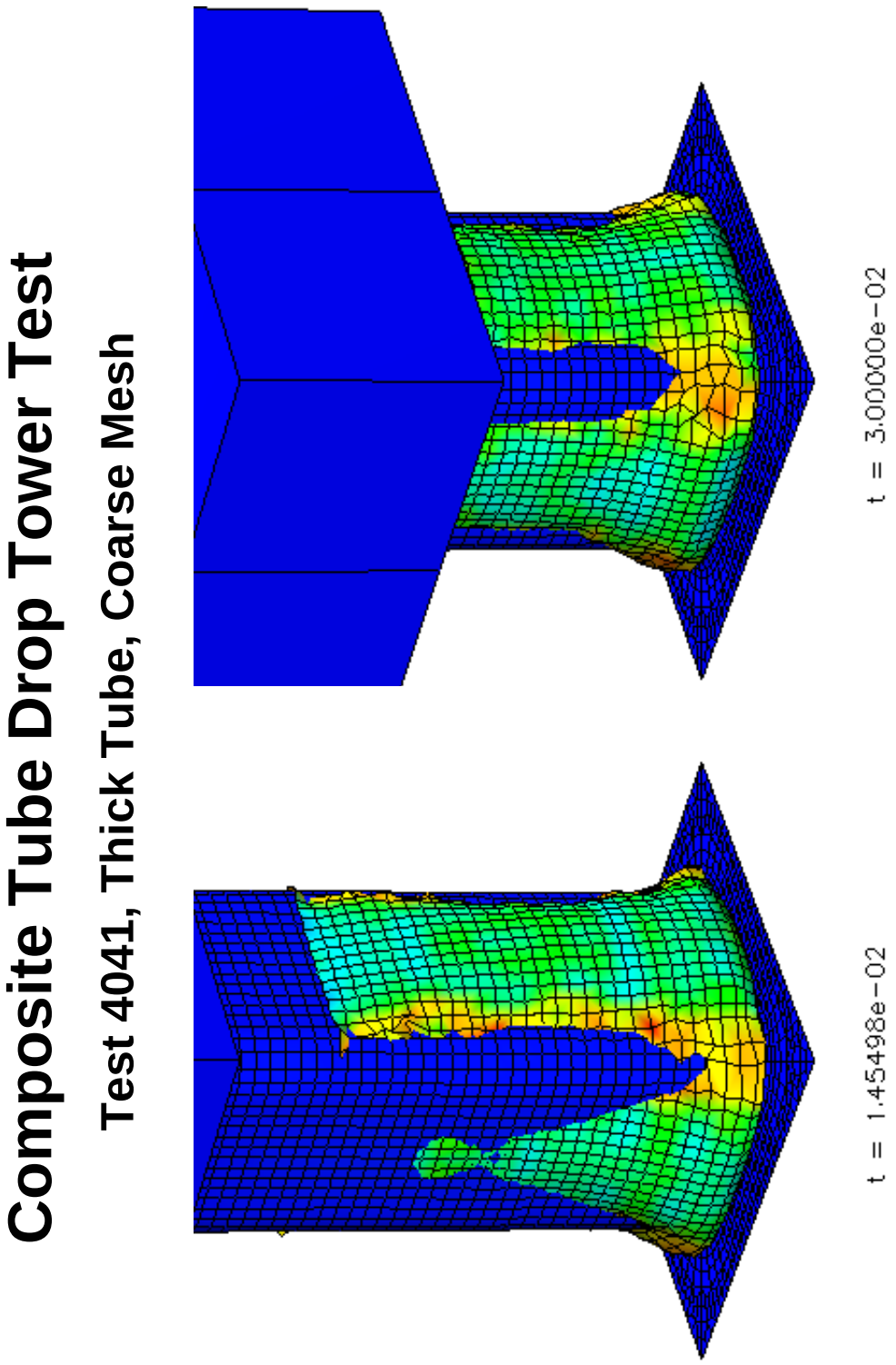

Figure 15. Material 53, Coarse Mesh, Deformation Sequence 2

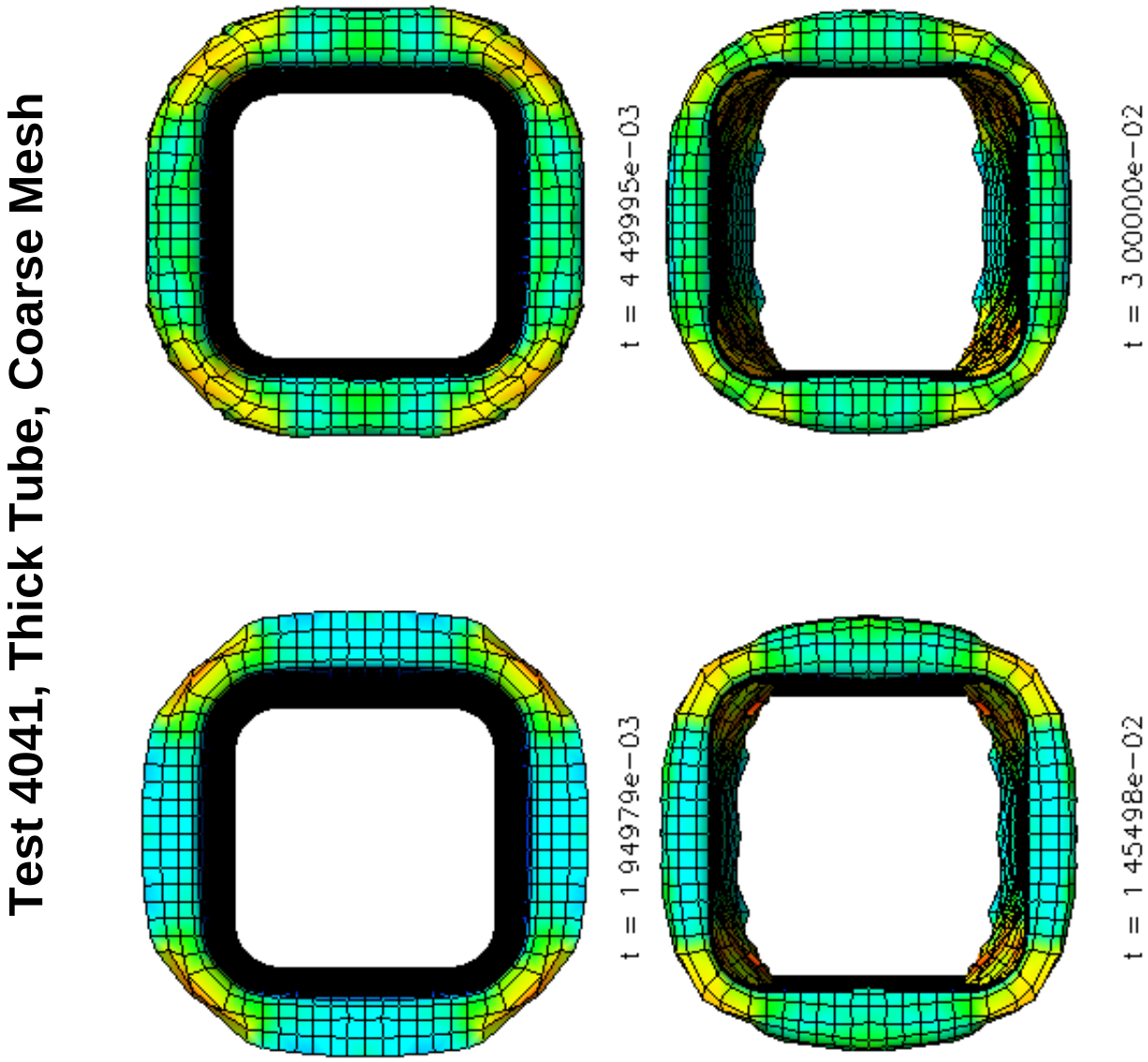

Figure 16. Material 53, Coarse Mesh, Bottom View

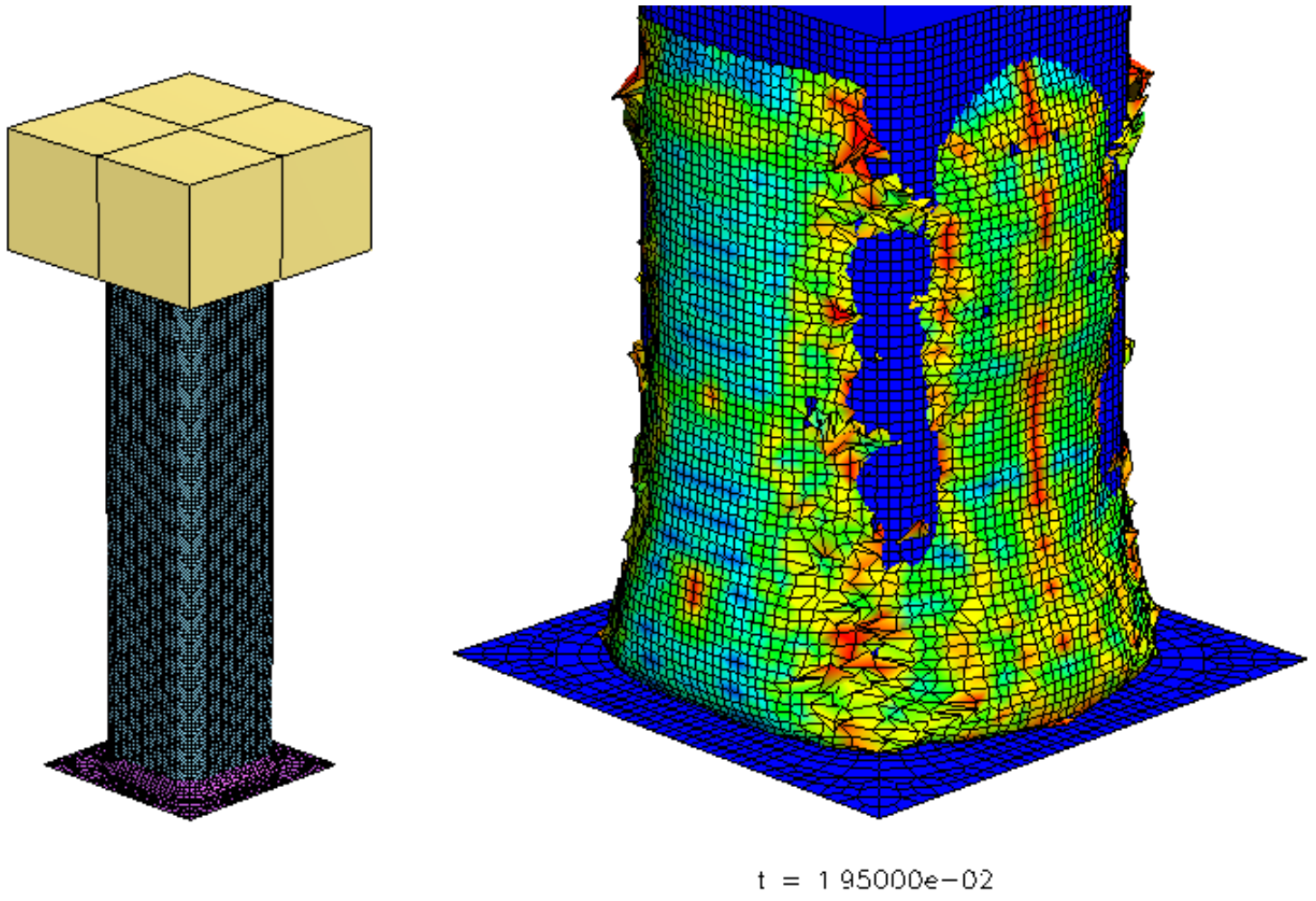

Figure 17. Material 53, Fine Mesh

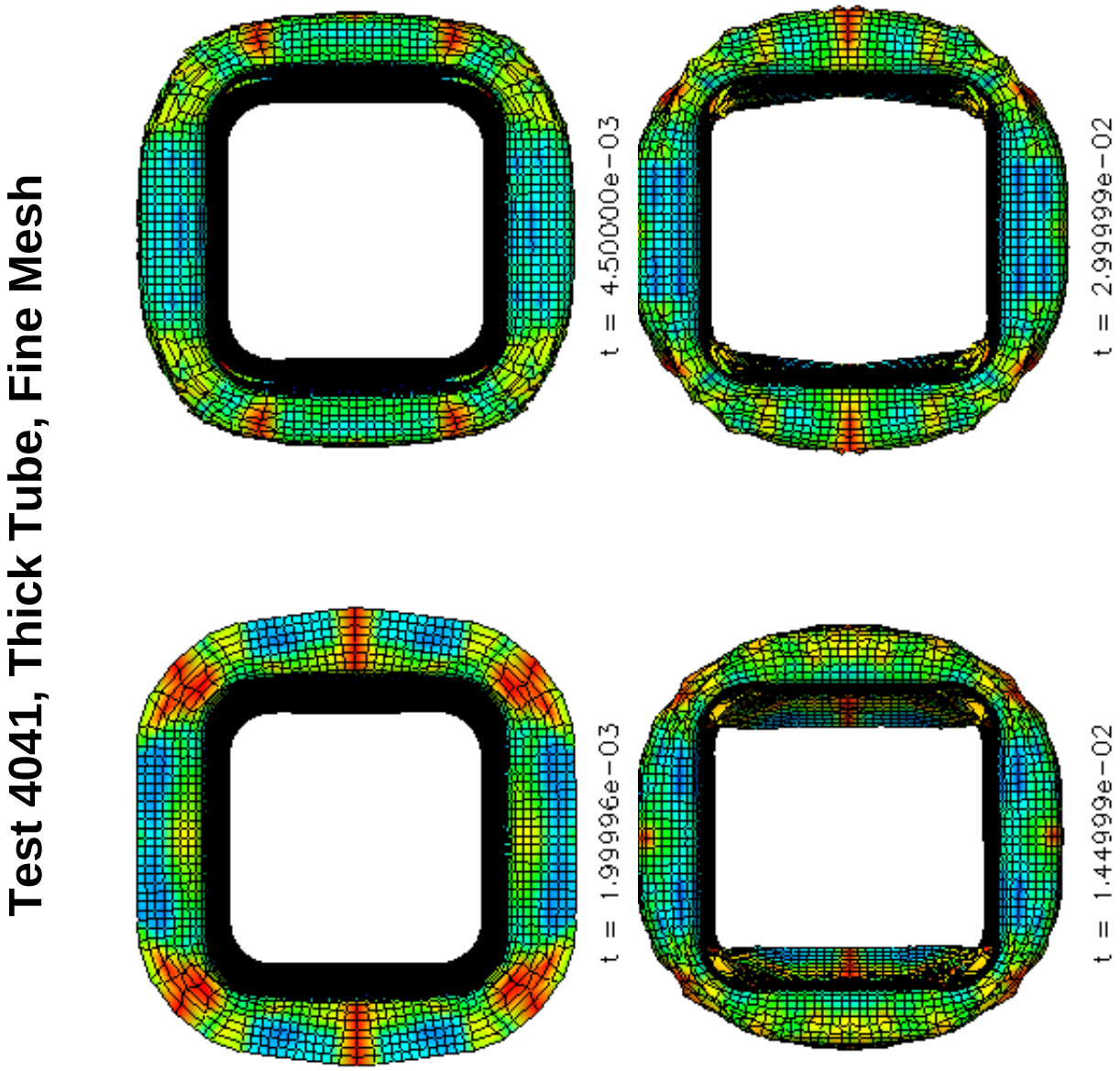

Figure 18. Material 53, Fine Mesh, Bottom View

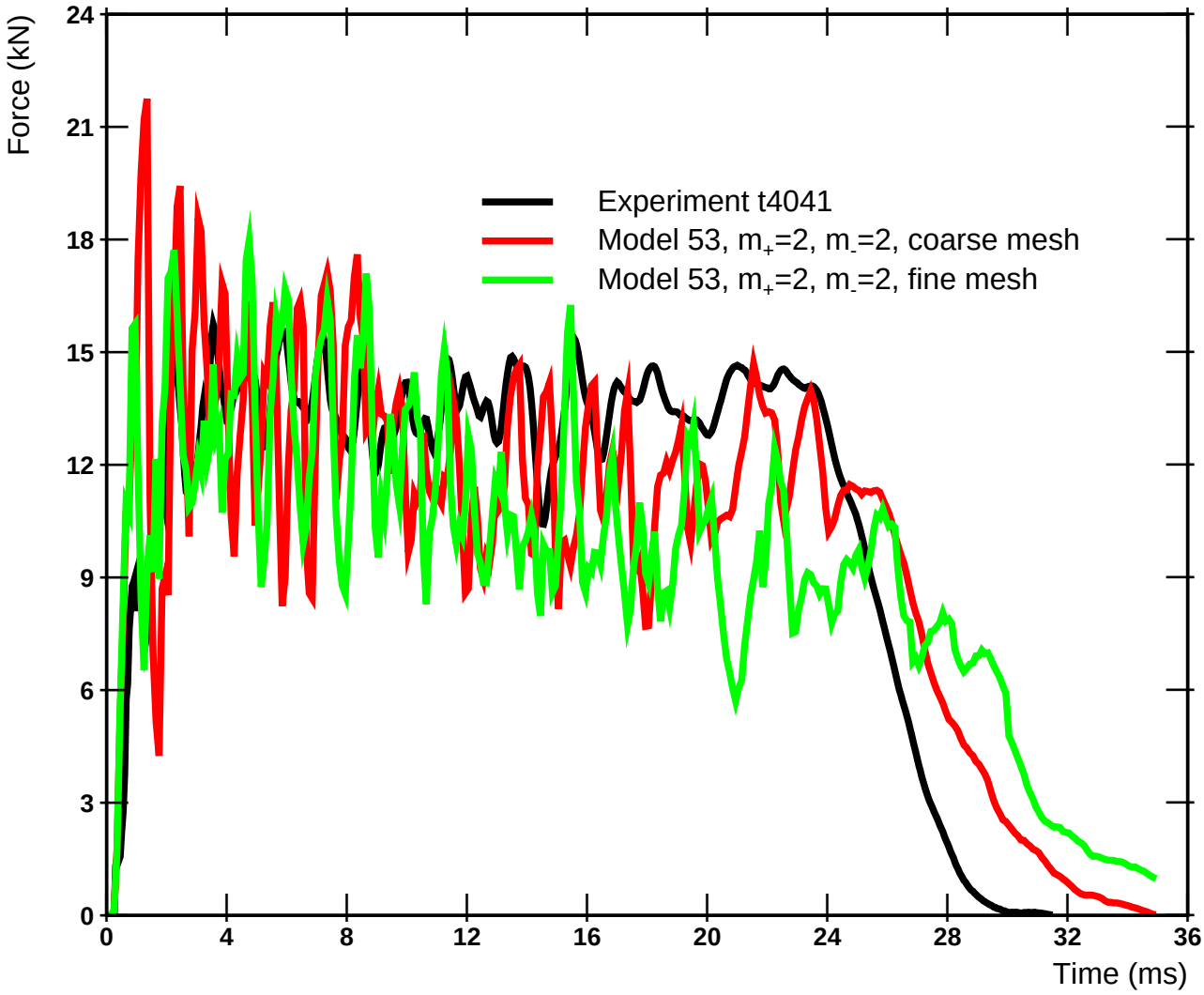

Figure 19. Material 53, Barrier Force

8. MATERIAL DATA INPUT FORMATS FOR DYNA3D

8.1. Material 52: Anisotropic Damage Model

The typical material card set for the anisotropic damage model is as follows:

```
    2   52 1.403E-06                                                  2
material type # 52  (user)
* ACC
*23456789+123456789+123456789+123456789+123456789+123456789+123456789+123456789+
*numc numh umcs umbk umsh umsf
   40    6   33   21    7    1
 14.40E+06 3.381E+06 3.381E+06    0.0245       0.3    0.0245 5.244E+060.7866E+06
0.7866E+060.1566E+060.1566E+060.6555E+06       3.0       0.5       2.0       0.5
       0.5       0.9       0.0       0.0 0.000E+00 0.000E+00 0.000E+00 0.000E+00
 0.000E+00 0.000E+00 0.200E-07 0.000E+00 0.000E+00 0.000E+00 0.000E+00 0.000E+00
 3.000E+00 0.000E+00 0.000E+00-1.000E+00 0.000E+00 0.000E+00 0.000E+00 0.000E+00
```

The first uncommented line contains the material identification number, material type, and its density. The second uncommented line is not to be changed except for the `umcs` parameter which denotes the location of the definition of the coordinate system for fiber orientation in the following five rows of the material cards. The coordinate system definition follows the rules outlined in the LLNL DYNA3D manual.[24] The parameters in the uncommented lines 3–7 are given schematically as

$E_\parallel$	$E_\perp$	E_{33}	ν_{21}	ν_{31}	ν_{32}	G	X_t
X_c	Y_t	Y_c	S	$m_{\parallel t}$	$m_{\parallel c}$	$m_{\perp t}$	$m_{\perp c}$
m_s	ω_{max}	0	0	0	0	0	0
0	0	Δt_{min}	μ	0	0	0	0
0	0	0	0	0	0	0	0

The parameters ω_{max} and Δt_{min} denote the maximum damage in either mode and the minimum time step for the element, respectively. All other parameters are as defined in Chap. 3.

8.2. Material 54: Hydrostatic Pressure Dependent Damage Model

The first material card denotes the material identification number, material type, and density of material. The second line need not be changed. The remaining five lines are organized as follows:

$N_{\epsilon(\omega)}$	I_{PL}	ν	ω_{max}	τ_+	τ_-	μ	I_H
ϵ_1	σ_1	...	...	...	...	ϵ_i	σ_i
...	...	ϵ_N	σ_N	ω_1	Y_1	...	...
...	...	ω_i	Y_i	...	...	ω_N	Y_N
0	0	0	0	0	0	0	Δt_{min}

The parameters that were not defined in Chap. 4 are

$N_{\epsilon(\omega)}$ – number of pairs defining (ϵ, σ) and (ω, Y) uniaxial loading curves

I_{PL} – material law indicator

0 – elastic–plastic–damage law

1 – elastic–damage law

ω_{max} – damage at failure

I_H – hardening indicator

0 – isotropic hardening

1 – kinematic hardening

(0,1) – mixed hardening (plastic law only)

Δt_{min}– minimum time step

A typical material card set for material model 54 is as follows:

```
    2   54 2.151E-06                                                    2
material type # 54  (user)
* ACC
*23456789+123456789+123456789+123456789+123456789+123456789+123456789+123456789+
*numc numh umcs umbk umsh umsf
   48    9    0   12   13    1
      6.00       1.00       0.32        0.4       1.00       0.00   0.0E-07       0.00
   0.00100 1.132E+04   0.00620 6.776E+04   0.00965 1.0376E+5   0.01313 1.212E+05
```

```
  0.02082  1.86E+05   0.03000 2.3606E+5        0.  1.132E+1     0.053  4.278E+2
    0.073  1.028E+3     0.089  1.884E+3    0.1063  3.422E+3      0.90 4.1415E+4
0.000E+00 0.000E+00 0.000E+00 0.000E+00 0.000E+00 0.000E+00 0.000E+00 0.000E+00
0.000E+00 0.000E+00 0.000E+00 0.000E+00 0.000E+00 0.000E+00 0.000E+00 0.200E-07
```

8.3. Material 53: Damage Model with Strain Tensor Split

The first material card denotes the material identification number, material type, and density of material. The second line needs not be changed. The remaining five lines are organized following the notation from Chap. 5 as follows:

E	ν	X_+	X_-	m_+	m_-	ω_{max}	Δt_{min}
0	0	μ	0	0	0	0	0
0	0	0	0	0	0	0	0
0	0	0	0	0	0	0	0
0	0	0	0	0	0	0	0
0	0	0	0	0	0	0	0

where ω_{max} and Δt_{min}, as before, denote the maximum damage and the minimum time step, respectively.

An example material card set for material model 53 is as follows:

```
    2   53 1.403E-06                                                    2
material type # 55  (user)
* ACC
*23456789+123456789+123456789+123456789+123456789+123456789+123456789+123456789+
*numc numh umcs umbk umsh umsf
   48   12    0    9   10    1
  11.0E+06      0.32  0.19E+06  0.22E+06      2.00      2.00      0.99   0.1E-06
 0.000E+00 0.000E+00 0.100E-04 0.000E+00 0.000E+00 0.000E+00 0.000E+00 0.000E+00
 0.000E+00 0.000E+00 0.000E+00 0.000E+00 0.000E+00 0.000E+00 0.000E+00 0.000E+00
 0.000E+00 0.000E+00 0.000E+00 0.000E+00 0.000E+00 0.000E+00 0.000E+00 0.000E+00
 0.000E+00 0.000E+00 0.000E+00 0.000E+00 0.000E+00 0.000E+00 0.000E+00 0.000E+00
 0.000E+00 0.000E+00 0.000E+00 0.000E+00 0.000E+00 0.000E+00 0.000E+00 0.000E+00
```

9. CONCLUSIONS

This report documents the development of computational models for continuous strand mat composite tube impact at the Oak Ridge National Laboratory. The models were developed during fiscal years 1994 through 1997 as a part of the Cooperative Research and Development Agreement, "Application of High–Performance Computing to Automotive Design and Manufacturing".

To illustrate the features and capabilities of the developed models, a tube crush experiment was simulated using each of the models. The experimental data were compared to the simulation results, and the advantages and deficiencies of the models were discussed. The model based on strain tensor split has shown very good agreement with physical experiments. Computational implementation of the developed models for the computer finite element code DYNA3D provide a practical platform for numerical simulation and analysis of impact of automotive composite structures.

The outcome of this research is very encouraging and shows that complex design problems for glass fiber reinforced composites can be addressed using computational modeling. These results easily surpass results presented in the current open literature and illustrate the considerable advancement in the theory of composite deformation achieved in the course of this project.

10. REFERENCES

1. Department of Energy. Application of high performance computing to automotive design and manufacturing. Oak Ridge National Laboratory, Statement of Work, CRADA Y1293-0188, 1993.

2. S. Simunovic and T. Zacharia. Application of high-performance computing to automotive design and manufacturing. Composite materials modeling task. Material properties of continuous strand mat composites. Technical Report ORNL/TM-13511, Oak Ridge National Laboratory, 1997.

3. S. Simunovic, Y. Zhu, and T. Zacharia. Application of high-performance computing to automotive design and manufacturing. Composite materials modeling task. Constitutive models for glass fiber-polymer matrix composites. Draft CRADA Report, Oak Ridge National Laboratory, 1996.

4. D. Krajcinovic. *Damage Mechanics*. Elsevier, 1996.

5. J. O. Hallquist, L. C. K. Lum, and A. Matzenmiller. Numerical simulation of post-failure dynamic crushing of composite tubular beams. Technical Report TR EM91-02, Automotive Composite Consortium, 1991.

6. A. de Rouvray and E. Haug. Failure of brittle and composite materials by numerical methods. In *Structural Failure, International Symposium on Structural Failure, Chapter 4*. MIT Press, 1988.

7. M. E. Botkin, N. L. Johnson, J. O. Hallquist, and A. Matzenmiller. Numerical simulation of post-failure dynamic crushing of composite tubes. In *2nd International LS-DYNA3D Conference*, 1994.

8. A. Matzenmiller, J. Lubliner, and R. L. Taylor. A constitutive model for anisotropic damage in fiber-composites. *Mechanics of Materials*, 20:125–152, 1995.

9. W. Weibull. A statistical distribution function of wide applicability. *Journal of Applied Mechanics*, 18:293–297, 1952.

10. D. Krajcinovic. Damage mechanics. *Mechanics of Materials*, 8:117–197, 1989.

11. P. Perzyna. Fundamental problems in visco-plasticity. In *Recent Advances in Applied Mechanics*, pages 244–368. Academic Press, 1966.

12. J. C. Simo, J. G. Kennedy, and S. Govindjee. Non-smooth multisurface plasticity and visco-plasticity loading/unloading conditions and numerical algorithms. *International Journal for Numerical Methods in Engineering*, 26:2161–2185, 1988.

13. G. Duvant and J. L. Lions. *Les inéquations en mécanique et en physique*. Dunod, Paris, 1972.

14. Y. Y. Zhu. *Contribution to the local approach of fracture in solid dynamics*. PhD thesis, University of Liege, 1992.

15. Y. Y. Zhu and S. Cescotto. A fully coupled elasto-visco-plastic damage theory for anisotropic materials. *International Journal of Solids and Structures*, 32:1607–1641, 1995.

16. Y. Y. Zhu, S. Cescotto, and A. M. Habraken. A fully coupled elasto-plastic damage modeling and fracture criteria in metalforming processes. *Journal of Materials Processing Technology*, 32:197–204, 1992.

17. P. Ladaveze. A damage computational method for composite structures. *Computers & Structures*, 44:79–87, 1992.

18. P. Ladaveze. Sur une théorie de l'endommagement anisotrope. Technical Report 34, Laboratorie de Mècanique de Technologie de Cachan, 1983.

19. J. O. Hallquist, D. W. Stillman, and T. L. Lin. LS-DYNA3D user's manual. Technical Report 1007, Livermore Software Technology Corporation, 1993.

20. V. A. Lubarda, D. Krajcinovic, and S. Mastilovic. Damage model for brittle elastic solids with unequal tensile and compressive strengths. *Engineering Fracture Mechanics*, 49:681–697, 1994.

21. P. Ladaveze, A. Gasser, and O. Allix. Damage mechanisms modeling for ceramic composites. *Journal of Engineering Materials and Technology*, 116:331–336, 1994.

22. DELSEN. Testing of CSM fiberglass material for tensile and compressive static/hysteresis properties. Technical Report T31665, DELSEN Testing Laboratories, 1995.

23. DELSEN. Testing of CSM fiberglass material for tensile and compressive static/hysteresis properties. Technical Report T31829-1, DELSEN Testing Laboratories, 1995.

24. R. G. Whirley and B. E. Engelmann. DYNA3D, a nonlinear, explicit, three-dimensional finite element code for solid and structural mechanics – user's manual. Technical Report UCRL-MA-107254 Rev. 1, Lawrence Livermore National Laboratory, 1993.

INTERNAL DISTRIBUTION

1–2. Central Research Library
3. Document Reference Section
4–5. Laboratory Records Department
6. Laboratory Records, ORNL PC
7. ORNL Patent Section
8–9. M&C Records Office
10. P. Angelini
11. R. A. Bradley
12. D. F. Craig
13. H. Gray
14. H. W. Hayden
15. G. M. Ludtka
16. B. Radhakrishnan
17. S. Simunovic
18. P. Sklad
19. D. Warren
20. T. Zacharia
21. R. E. Zeigler

EXTERNAL DISTRIBUTION

22. DOE, OAK RIDGE OPERATIONS, P.O. Box 2001, Oak Ridge, TN 37831-6269

23. DOE, OFFICE OF HEAVY VEHICLE TECHNOLOGY, VEHICLE MATERIALS TECHNOLOGY PROGRAM, EE-RE, Forrestal Building, 1000 Independence Avenue S.W., Washington, DC 20585
S. Diamond

24. DOE, OFFICE OF ADVANCED AUTOMOTIVE TECHNOLOGIES, LIGHTWEIGHT VEHICLE MATERIALS, EE-32, Forrestal Building, 1000 Independence Avenue S.W., Washington, DC 20585
T. Marechaux

25. CHRYSLER CORPORATION, 800 Chrysler Drive, East Auburn Hills, MI 48326-2757
Sukhbir Bilkhu

26. CHRYSLER CORPORATION, CIMS 483-05-10, 800 Chrysler Drive, East Auburn Hills, MI 48326-2757
Venkatesh Agaram

27. FORD MOTOR COMPANY, Village Plaza, Suite 800, 23400 Michigan Avenue, Dearborn, MI 48124
Richard Jeryan

28. FORD MOTOR COMPANY, Village Plaza, Suite 800, 23400 Michigan Avenue, Dearborn, MI 48124
Hikmat F. Mahmood

29. GENERAL MOTORS, 30500 Mound Road, P. O. Box 9055 Warren, MI 48090-9055
Mark Botkin

30. GENERAL MOTORS, 30500 Mound Road, P. O. Box 9055 Warren, MI 48090-9055
Nancy Johnson